Annals of Physics 412 (2020) 168045

Contents lists available at ScienceDirect

Annals of Physics

journal homepage: www.elsevier.com/locate/aop

Kramers' escape rate problem within a non-Markovian description

Benjamin Schüller [a,*], Alex Meistrenko [a], Hendrik van Hees [a], Zhe Xu [b], Carsten Greiner [a]

[a] Institut für Theoretische Physik, Goethe-Universität Frankfurt am Main, Max-von-Laue-Straße 1, 60438 Frankfurt am Main, Germany
[b] Department of Physics, Tsinghua University and Collaborative Innovation Center of Quantum Matter, Beijing 100084, China

ARTICLE INFO

Article history:
Received 4 June 2019
Accepted 23 November 2019
Available online 29 November 2019

Keywords:
Generalized Langevin equation
Kramers' escape rate
Colored noise
Non-Markovian dynamics

ABSTRACT

We compare the thermal escape rates of a Brownian particle, initially trapped into one of the two wells of an asymmetric double-well potential, for thermal Markovian and non-Markovian noise. The Markovian treatment of this problem goes originally back to the studies of Kramers in 1940 and is therefore often referred to as "Kramers' escape rate problem". We solve the generalized Langevin equation for the trajectories of the particles numerically and analytically for both limiting cases, Markovian and non-Markovian thermal noise. We compute the escape rate and work out the fundamental differences arising from finite correlation times of the thermal noise.

1. Introduction

Since the seminal development of the theory of Brownian motion by Einstein [1] and Langevin's formulation in terms of a stochastic process [2,3] this framework has found applications in a very broad range of fields of physics, chemistry, engineering, and finance mathematics [4]. Of particular interest are also semi-classical descriptions of the dynamics of open quantum systems [5–7] and non-equilibrium relativistic quantum field theory with applications in (inflationary) cosmology and

* Corresponding author.
E-mail addresses: schueller@th.physik.uni-frankfurt.de (B. Schüller), meistrenko@th.physik.uni-frankfurt.de (A. Meistrenko), hees@th.physik.uni-frankfurt.de (H. van Hees), xuzhe@mail.tsinghua.edu.cn (Z. Xu), Carsten.Greiner@th.physik.uni-frankfurt.de (C. Greiner).

https://doi.org/10.1016/j.aop.2019.168045
0003-4916/

the early universe like thermalization, decoherence and structure formation (see e.g. Ref. [8] and references within) and with applications in the description of the hot and dense strongly interacting matter as created in ultrarelativistic heavy-ion collisions like the Markovian and non-Markovian dynamics of disoriented chiral condensates, heavy quarks, the chiral phase transition, and baryon diffusion [8–22].

The general concept of a Brownian particle initially trapped in a metastable state and being able to escape from it via thermally activated fluctuations can describe a large variety of phenomena from different fields of science as for example the transport of electrons in semiconductors, the diffusion of impurities bound in a harmonic lattice, biophysical transport problems like the migration of ligands in biomolecules, and chemical reactions [23–25]. After an empirical analysis of various reaction-rate data in the late 19th century Svante Arrhenius concluded that the rate of escape out of the metastable state obeys the following law:

$$k = \nu \exp\left[-\frac{E_\mathrm{b}}{k_\mathrm{B}T}\right], \tag{1}$$

where ν is some prefactor, which will be specified later in the course of this work, E_b is the energy the Brownian particle must attain to escape, k_B is the Boltzmann constant, and T denotes the temperature. In the literature this general result for the rate of escape from a metastable state is referred to as Van't Hoff–Arrhenius law [26–28]. It should be noted here that in this work the temperature remains constant during the evolution of the system as the thermal bath, the Brownian particle is exposed to, is assumed to be in thermodynamic equilibrium. Subsequently, investigators tried to determine the actual form of the prefactor ν in Eq. (1) using different approaches. One of them was Hendrik Antonie Kramers in 1940 in his work on a diffusion model of chemical reactions [29].

This work, based on B.S.'s Master's thesis [30], is precisely focused on this diffusion model dealing with the thermally activated rate of escape of a Brownian particle initially trapped in a potential well. Kramers' classical model, characterized by a Markovian thermal noise, will be extended to the case of non-Markovian thermal noise terms. Thereby, the main objectives will be computing Kramers' escape rate for Markovian and non-Markovian noise numerically as a function of the damping rate β and working out the differences between these two cases. Furthermore, an attempt will be made to explain the occurring differences.

To this end, the generalized Langevin equation (GLE), Eq. (40), is solved for an asymmetric double-well potential using a Markovian and three non-Markovian thermal noise variants.

This work is organized as follows. In Section 2 the algorithm for the generation of non-Markovian noise used for the numerical simulations in this work is presented.

Section 3 is devoted to Kramers' diffusion model. Besides the classical model, also extensions to it will be introduced, before analytical results for the escape rate of the Markovian and one of the non-Markovian thermal noise variants are reviewed.

Thereafter, Section 4 addresses the detailed numerical simulations and the comparison of numerical with analytical results. After presenting the actual numerical setup, Kramers' escape rate as a function of the damping rate is presented for different correlation functions and correlation times.

Finally, in Section 5 the results of this work are summarized. These results and methods are applicable in various physical surroundings, however, motivated by high energy nuclear and particle physics natural units are used, $\hbar = c = k_\mathrm{B} = 1$ and $\mathrm{fm\,GeV} = 0.197^{-1}$.

2. Generating colored noise

This section is devoted to the method for the generation of stationary Gaussian colored noise the numerical simulations of this work are based on. The method was developed in Ref. [14] and recently employed in Ref. [31], where a detailed instruction for the numerical implementation of this method is indicated as well.

It is worth mentioning that the two terms white and colored noise, which will be frequently used in the further course of this work, correspond to Markovian and non-Markovian noise, respectively.

That terminology originates from considerations concerning the spectral density of the correlation function of the stationary Gaussian noise. While the spectral density is constant for a δ-correlated Markovian noise, it is dependent on the frequency for non-Markovian noise [32].

Before the actual method is presented, several preliminary considerations are needed. The starting point is a very general expression for a centered, stochastic process $\xi(t)$ which consists of n random pulses in a time interval $[0, T']$ [33]:

$$\xi(t) = \sum_{i=1}^{n} a_i b(t - t_i), \quad t \in [0, T'], \tag{2}$$

where $\langle \xi(t) \rangle = 0 \Leftrightarrow \langle a_i \rangle = 0$. While n, a_i, and t_i denote random variables, $b(t)$ designates an arbitrary pulse shape. The number of pulses in the time interval $[0, T']$ is supposed to be Poisson-distributed with mean $\bar{n} = \mu T'$, whereby μ identifies with the mean rate of pulses in $[0, T']$. Furthermore, a_i is the random height of the ith pulse, and t_i the random instant of time for the occurrence of a pulse.

The next step is to find an expression for white noise. Since white noise is δ-correlated, a reasonable choice for the pulse shape $b(t)$ of white noise is [31]

$$b(t) = \sqrt{\frac{D}{\mu \sigma^2}} \delta(t), \tag{3}$$

where D is an arbitrary positive real number whose meaning will later be specified in a physical context, and σ^2 denotes the variance of the pulse height a_i. With this pulse shape for white noise the corresponding centered stochastic process $\xi_{\mathrm{w}}(t)$, where the subscript stands for white, reads

$$\xi_{\mathrm{w}}(t) = \sqrt{D} \bar{\xi}_w(t), \tag{4}$$

where

$$\begin{aligned} \bar{\xi}_w(t) &= \sum_{i=1}^{n} \frac{a_i}{\sigma \sqrt{\mu}} \delta(t - t_i) \\ &= \sum_{i=1}^{n} \frac{\bar{a}_i}{\sqrt{\mu}} \delta(t - t_i), \quad \bar{a}_i := \frac{a_i}{\sigma}. \end{aligned} \tag{5}$$

In the limit of a large rate of pulses μ ($\mu \to \infty$) and a small variance σ^2 of the distribution function $p(a)$ of the pulse height ($\sigma^2 \to 0$), the δ-correlated white stochastic process becomes Gaussian [14]. It should be noted that by use of the central limit theorem the distribution function for a_i is optional and by definition of the white noise (4) the prefactor D of the pulse shape $b(t)$ (3) is identified with the strength of the fluctuative force from the classical Langevin equation (LE) (see Ref. [32]).

A centered Gaussian process is uniquely determined by its first two moments:

$$\langle \xi(t) \rangle = 0, \tag{6}$$

$$\left\langle \xi(t) \xi(t') \right\rangle = \mu \sigma^2 \int_0^{T'} b(t - s) b(t' - s) \mathrm{d}s := C(t, t'). \tag{7}$$

For the following considerations the correlation function $C(t, t')$ of the Gaussian process needs to be stationary, meaning the correlation function shall not be dependent on the times t and t' separately but on the time difference $|t - t'|$, i.e. $C(t, t') = C(|t - t'|)$ [31]. This can be attained by demanding a symmetric correlation function [31]. In what follows the purpose is to determine the pulse shape $b(t)$ of a stationary Gaussian process, given a stationary correlation function. By use of the Wiener–Khinchin theorem, stating that the spectral density $S_\xi(\omega)$ of a stationary process is obtained by the Fourier transform of its correlation function $C(t, t')$ [32], one arrives at

$$S_\xi(\omega) = \mathcal{F}[C] = \mu \sigma^2 |\tilde{b}(\omega)|^2. \tag{8}$$

Without loss of generality, $\tilde{b}(\omega)$ is set to be real and positive ($\tilde{b}(\omega) \geq 0$, $\forall \omega \in \mathbb{R}$). In this way Eq. (8) can be simply solved for $\tilde{b}(\omega)$. Subsequent back-transform of $\tilde{b}(\omega)$ leads to

$$\tilde{b}(\omega) = \frac{1}{\sigma\sqrt{\mu}}\sqrt{S_\xi(\omega)}, \tag{9}$$

$$\Rightarrow b(t) = \mathcal{F}^{-1}\left[\tilde{b}(\omega)\right](t) = \frac{1}{\sigma\sqrt{\mu}}G(t), \quad G(t) = \mathcal{F}^{-1}\left[\sqrt{S_\xi(\omega)}\right](t). \tag{10}$$

From this, the general expression for a stationary Gaussian process (see Eq. (2)) is readily transformed into the following form, using the definition (4) of a Gaussian white noise and relation (10) for $b(t)$

$$\begin{aligned}\xi(t) &= \sum_{i=1}^{n} a_i b(t-t_i) \\ &= \sum_{i=1}^{n}\int_{-\infty}^{\infty} a_i b(t-t')\delta(t'-t_i)\mathrm{d}t' = \int_{-\infty}^{\infty} b(t-t')\sum_{i=1}^{n} a_i\delta(t'-t_i)\mathrm{d}t' \\ &= \int_{-\infty}^{\infty} b(t-t')\sigma\sqrt{\mu}\bar{\xi}_w(t')\mathrm{d}t' = \int_{-\infty}^{\infty} G(t-t')\bar{\xi}_w(t')\mathrm{d}t'.\end{aligned} \tag{11}$$

Hence, the method for generating stationary Gaussian colored noise, described in this section, is primarily based on the determination of the underlying pulse shape $b(t)$ of a stationary correlation function $C(|t-t'|)$ and the subsequent convolution of this pulse shape $b(t)$ with a sequence of δ-correlated Gaussian white noise $\xi_w(t)$.

In the course of this work various correlation functions are investigated which are listed below together with their corresponding Fourier transforms,

$$C_1(|t|) := \langle\xi(t)\xi(0)\rangle = \frac{D}{2\tau}\exp\left[-\frac{|t|}{\tau}\right], \tag{12}$$

$$C_2(|t|) := \langle\xi(t)\xi(0)\rangle = \frac{D}{a\sqrt{\pi}}\exp\left[-\left(\frac{|t|}{a}\right)^2\right], \tag{13}$$

$$C_3(|t|) := \langle\xi(t)\xi(0)\rangle = \frac{g}{4}k_\mathrm{B}T\alpha^2\left(1-\frac{\alpha}{\sqrt{m}}|t|\right)\exp\left[-\frac{\alpha}{\sqrt{m}}|t|\right], \tag{14}$$

and

$$\mathcal{F}[C_1] := \frac{D}{1+\tau^2\omega^2}, \tag{15}$$

$$\mathcal{F}[C_2] := D\exp^{-\frac{\alpha^2\omega^2}{4}}, \tag{16}$$

$$\mathcal{F}[C_3] := \frac{gk_\mathrm{B}T\alpha^3\omega^2}{\sqrt{m}\left(\omega^2+\frac{\alpha^2}{m}\right)^2}, \tag{17}$$

where α is given by relation (C.3), g is a dimensionless coupling constant (see Appendix C), and the following convention for the Fourier transform has been employed

$$\Gamma(t) = \frac{1}{2\pi}\int_{-\infty}^{\infty} e^{-\mathrm{i}\omega t}\tilde{\Gamma}(\omega)\mathrm{d}\omega, \tag{18}$$

$$\tilde{\Gamma}(\omega) = \int_{-\infty}^{\infty} e^{\mathrm{i}\omega t}\Gamma(t)\mathrm{d}t. \tag{19}$$

For these correlation functions evidence of the validity of the indicated method is given in Fig. 1. Herein, the correlation of the colored noise $\langle\xi(t)\xi(0)\rangle$, obtained by numerically averaging an ensemble of particle trajectories , is compared to the appropriate analytical expression of the

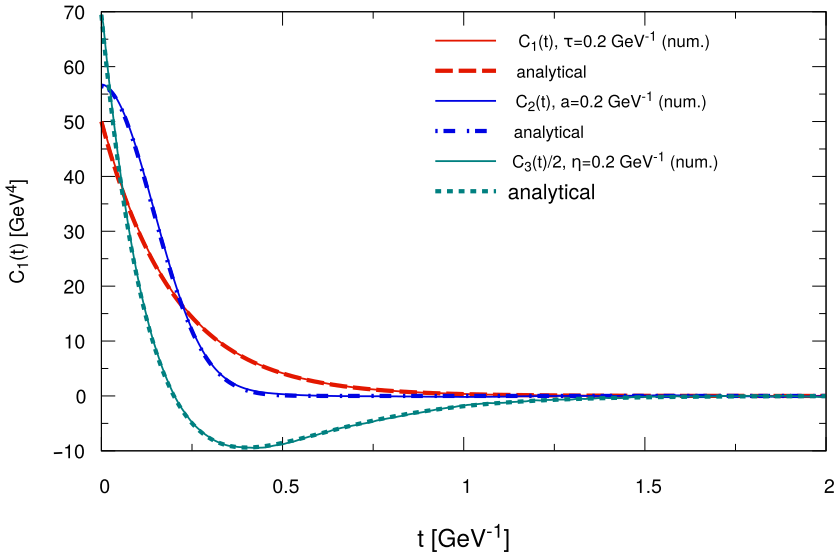

Fig. 1. Comparison of the numerical correlations $\langle \xi(t)\xi(0)\rangle$ for C_1, C_2, and C_3 (red, blue, and green line), averaged over $8 \cdot 10^5$ runs, with the appropriate analytical expressions (12)–(14) (red long dashed line, blue dashed/dotted line, green small dashed line), where $m = 1.11\,\mathrm{GeV}$, $T = 1\,\mathrm{GeV}$, $D = 20\,\mathrm{GeV}^3$ for correlation functions $C_1(t)$ and $C_2(t)$, and $g = 20$ for correlation function $C_3(t)$. The time is given in units of GeV^{-1} and can be converted to fm by means of relation $\mathrm{fm\,GeV} = 0.197^{-1}$. (For interpretation of the references to color in this figure legend, the reader is referred to the web version of this article.)

correlation function. The first two correlation functions, C_1 and C_2, do have an immediate intuitive interpretation, the first being an exponential decay and the second being a Gaussian distribution. The interpretation of the third correlation function C_3 is not as trivial. Obviously, C_3 becomes slightly negative in the past time, and the Fourier transform of C_3 vanishes for $\omega \to 0$. Such a dissipative kernel is rather typical in a quantum field theoretical setting in a self-interacting theory like a scalar Φ^4-theory (see e.g. Ref. [14]). Some peculiarities of this particular correlation function C_3 are given in Appendix C where for a free Brownian motion no full thermalization is observed.

3. Kramers' escape rate problem

3.1. Classical model

In 1940 Kramers established a model for chemical reactions in his paper on "Brownian motion in a field of force and the diffusion model of chemical reactions" (see Ref. [29]). Herein, Kramers describes a chemical reaction by two metastable states divided by an intermediate state. The transition from one to the other state shall be thermally activated. This situation is then approximated by a classical Brownian particle of mass m inside a one-dimensional, asymmetric double-well potential [28,29] (see Fig. 2). The two metastable states, corresponding in this model to the two wells of the asymmetric double-well potential, constitute the reactant and product state located at x_a and x_c, respectively. The intermediate state, represented by the maximum of the barrier between these two wells at $x = x_b$, is designated as transition state [28]. The position coordinate x of the particle, describing the course of a chemical reaction, is fittingly referred to as reaction coordinate [28]. Furthermore, the Brownian particle moving in the potential $V(x)$ is thought to be surrounded by a thermal environment in form of a heat bath at temperature T. This heat bath, constituting a stochastic force $\xi(t)$ and a friction force $F_r = -\gamma v$, has to be understood as a consequence of the residual degrees of freedom of the system [28]. The appropriate LE, describing the above

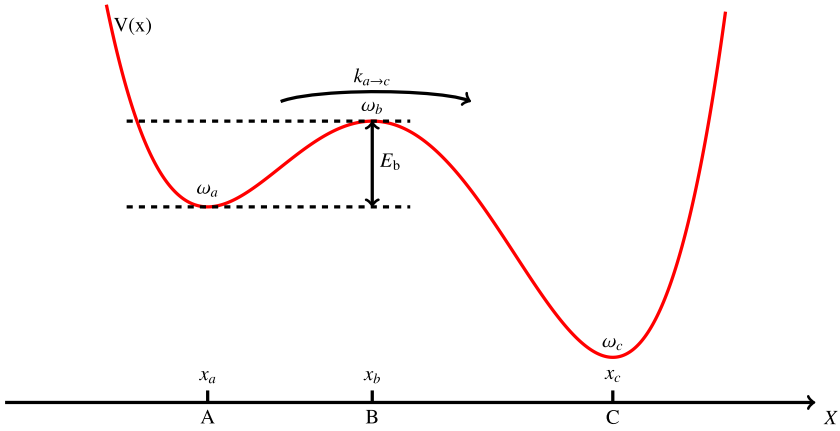

Fig. 2. Asymmetric double-well potential $V(x)$ of Kramers' classical escape rate problem, consisting of the A-well with frequency ω_a located around x_a and the C-well with frequency ω_c located around x_c. Both wells are separated by a barrier around x_b with barrier height E_b and frequency ω_b.
Source: Original figure from Ref. [28].

characterized dynamics of the Brownian particle, is given by the classical LE complemented by the external potential field $V(x)$,

$$\begin{aligned}\dot{x} &= v,\\ \dot{v} &= -\frac{1}{m}\frac{dV(x)}{dx} - \beta v + \frac{\xi}{m}, \quad \langle\xi(t)\rangle = 0, \quad \langle\xi(t)\xi(0)\rangle = D\delta(t),\end{aligned} \tag{20}$$

where $\xi(t)$ denotes a centered, δ-correlated and Gaussian-distributed noise, and $\beta = \gamma/m$. The strength D of the stochastic force $\xi(t)$ and β in Eq. (20) are linked by the fluctuation–dissipation relation,

$$\beta = \frac{\gamma}{m} = \frac{D}{2k_B T m}, \tag{21}$$

which states that both frictional and stochastic force originate from the same source.

Dealing with an ergodic system, Kramers considers an ensemble of particles, meaning an entirety of many similar particles, all evolving independently from each other [29]. Each of these particles is supposed to be initially trapped in the potential well near the reactant state x_a. Induced by many subsequent, thermally activated collisions with the solvent molecules, constituting the thermal environment, the Brownian particle will potentially, yet rarely, be able to surmount the potential barrier at some point.

Kramers' escape rate problem is then to determine the probability for this Brownian particles to overcome the barrier whereby the barrier height E_b is supposed to be large compared to the energy $E_\mathrm{th} = k_\mathrm{B}T$ supplied by the thermal bath [29]:

$$k_\mathrm{B}T \ll E_\mathrm{b}. \tag{22}$$

In this way, the Brownian particle will thermalize before escaping from the initial well. Condition (22), furthermore, leads to a clear-cut separation of time scales for $\tau_a := 2\pi\omega_a^{-1}$ and the escape time $\tau_e \approx \tau_a \exp\left[\frac{E_\mathrm{b}}{k_\mathrm{B}T}\right] \gg \tau_a$, which always needs to hold when dealing with rate problems [28]. Since under this condition the escape from the initial well is very slow, Kramers assumes the diffusion process to be quasi-stationary [29] which will be important for later calculations (see Section 3.3).

Thus, the quasi-stationary current from the initial well over the barrier is given by the probability rate for the Brownian particles to leave the well, $k_{A\to C}$, multiplied with the number of particles, n_a,

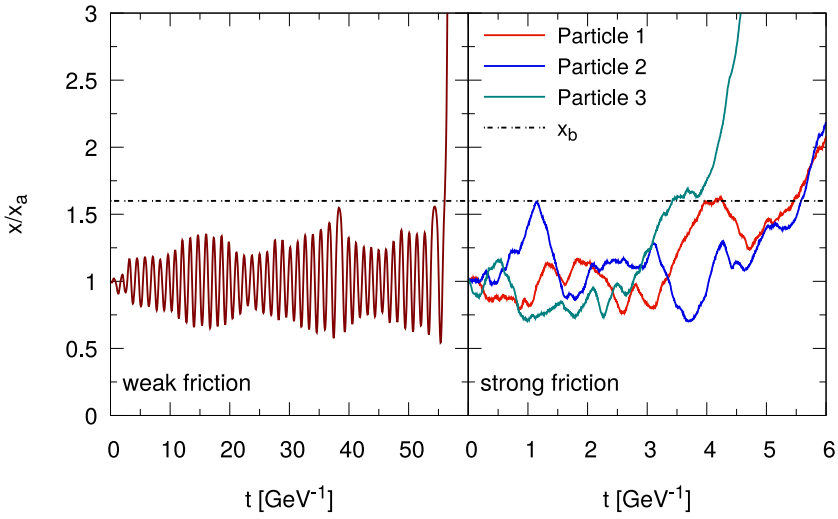

Fig. 3. Position as a function of time for several Brownian particles and Markovian noise, Eq. (132), moving in the potential V(x), Eq. (130), where $E_\mathrm{b} = 2.5\,\mathrm{GeV}$, $\omega_b = 5\,\mathrm{GeV}$, $m = 1.11\,\mathrm{GeV}$, $T = 1\,\mathrm{GeV}$, $\beta = 0.03375\,\mathrm{GeV}$ in the (very) weak- (left figure) or $\beta = 9\,\mathrm{GeV}$ in the strong-friction regime (right figure), and x_a denotes the initial position of the Brownian particle, respectively. The above-mentioned potential V(x) is depicted in Fig. 6, where the barrier top is located at $x_b = 1.6x_a$.

being located in this well [29]:

$$j_b = k_{A\to C} n_a. \tag{23}$$

The coupling strength of the considered Brownian particles, the thermal bath, and potential other degrees of freedom are completely determined by the friction coefficient β [28]. Depending on its actual value Kramers differentiates between two regimes, the weak- and strong-friction regime [29]. While the weak-friction regime is governed by an almost frictionless oscillation of the respective Brownian particle in the bottom of the well, the high-friction regime is determined by the spatial diffusive dynamics of the Brownian particle around the barrier top [28,29].

To visualize the processes connected to the different limiting regimes, Fig. 3 shows typical trajectories of several Brownian particles, one for weak and three for strong friction, being subjected to an asymmetric double-well potential (see Figs. 2 and 6). Note that not only the shape of the curves but also the time scale of escape, i.e. the time that elapses until a Brownian particle crosses the barrier located at x_b, is significantly different for both limiting regimes.

In the weak-friction regime a particle oscillating in the A-well loses almost no energy due to friction loss during the time of an oscillation [29]. The energy loss ΔE in this limiting regime can be expressed in terms of the action I [28],

$$\Delta E = \beta I(E), \tag{24}$$

where $I(E)$ defines the action at energy E given by

$$I(E) = \oint p\mathrm{d}x. \tag{25}$$

Using relation (24) the weak-friction regime occurs whenever the energy loss during an oscillation is much smaller than the thermal energy provided by the heat bath [28], i.e.

$$\beta I(E) \ll k_\mathrm{B} T. \tag{26}$$

A particle eventually reaching the barrier top by successive accumulation of small amounts of energy will relax towards the C-well. Hence, in this limiting regime the rate of escape is controlled

by energy diffusion [28], described by the following diffusion equation [28,29]:

$$\frac{\partial P(E,t)}{\partial t} = \beta \frac{\partial}{\partial E} I(E) \left[1 + k_\mathrm{B} T \frac{\partial}{\partial E} \right] \frac{\omega(E)}{2\pi} P(E,t). \tag{27}$$

This diffusion equation can be derived by performing a canonical transformation from position and momentum coordinates to action and angle coordinates, $(x,p) \to (I,\phi)$, and subsequently averaging over the angle ϕ to obtain the diffusion equation for the probability density of the action, starting from the Klein–Kramers equation [28,29],

$$\frac{\partial P(I,t)}{\partial t} = \beta \frac{\partial}{\partial I} I \left[1 + \frac{2\pi k_\mathrm{B} T}{\omega(I)} \frac{\partial}{\partial I} \right] P(I,t). \tag{28}$$

Thereby, energy and action are related through the angular frequency $\omega(I)$ by [28]

$$\frac{\partial E}{\partial I} = \frac{\omega(I)}{2\pi}. \tag{29}$$

Using relation (29) differential Eq. (28) is readily transferred into the appropriate differential equation for the energy, Eq. (27). The corresponding steady-state escape rate $k_{A\to C}$ is then given by [28]

$$k_{A\to C} = \beta \frac{I(E_\mathrm{b})}{k_\mathrm{B} T} \frac{\omega_a}{2\pi} \exp\left[-\frac{E_\mathrm{b}}{k_\mathrm{B} T} \right], \quad \beta \to 0, \quad \frac{k_\mathrm{B} T}{E_\mathrm{b}} \ll 1, \quad \beta I(E_\mathrm{b}) \ll k_\mathrm{B} T. \tag{30}$$

Gradually increasing the damping rate β finally leads to a point where condition (26) is no longer valid. This limit, which is characterized by the fact that the energy loss ΔE during the time of an oscillation is greater than the thermal energy, i.e.

$$\beta I(E) > k_\mathrm{B} T, \tag{31}$$

is referred to as intermediate-to-strong-friction regime [28]. Here, the rate-determining mechanism is the dynamics around the top of the barrier and the escape becomes controlled by spatial diffusion, described by the Klein-Kramers equation [32],

$$\frac{\partial P(x,v,t)}{\partial t} = \left[-v \frac{\partial}{\partial x} - \frac{\partial}{\partial v} \left(-\frac{\gamma}{m} v - \frac{V'(x)}{m} \right) + \frac{D}{2m^2} \frac{\partial^2}{\partial v^2} \right] P(x,v,t), \tag{32}$$

which is a special Fokker–Planck equation (FPE). Hereby, it should be emphasized that a particle crossing the top of the barrier x_b will not necessarily be trapped into the neighboring well. Instead, it can recross the barrier again and will, therefore, reduce the escape rate.

The steady-state escape rate in the intermediate-to-strong-friction regime, which will be explicitly derived in Section 3.3, is given by [28]:

$$k_{A\to C} = \frac{\lambda_\mathrm{M}}{\omega_b} \frac{\omega_a}{2\pi} \exp\left[-\frac{E_\mathrm{b}}{k_\mathrm{B} T} \right], \quad \beta I(E_\mathrm{b}) > k_\mathrm{B} T, \tag{33}$$

where

$$\lambda_\mathrm{M} = \sqrt{\frac{\beta^2}{4} + \omega_b^2} - \frac{\beta}{2}, \tag{34}$$

and the subscript M denotes the classical Markovian case. The expression (34) for the quantity λ_M will be motivated later (see Section 3.3). For large damping rates β, that is $\beta \gg \omega_b$, Eq. (33) can be expanded with respect to $x := \frac{\omega_b}{\beta}$ around $x \approx 0$, yielding

$$k_{A\to C} = \frac{\omega_b}{\beta} \frac{\omega_a}{2\pi} \exp\left[-\frac{E_\mathrm{b}}{k_\mathrm{B} T} \right], \quad \beta \to \infty. \tag{35}$$

Altogether, it is to be stated that concerning β there are two limiting regimes, the weak- and the strong-friction regime, whereby the escape rate $k_{A\to C}$ is proportional to β in the weak- and inversely proportional to β in the strong-friction regime.

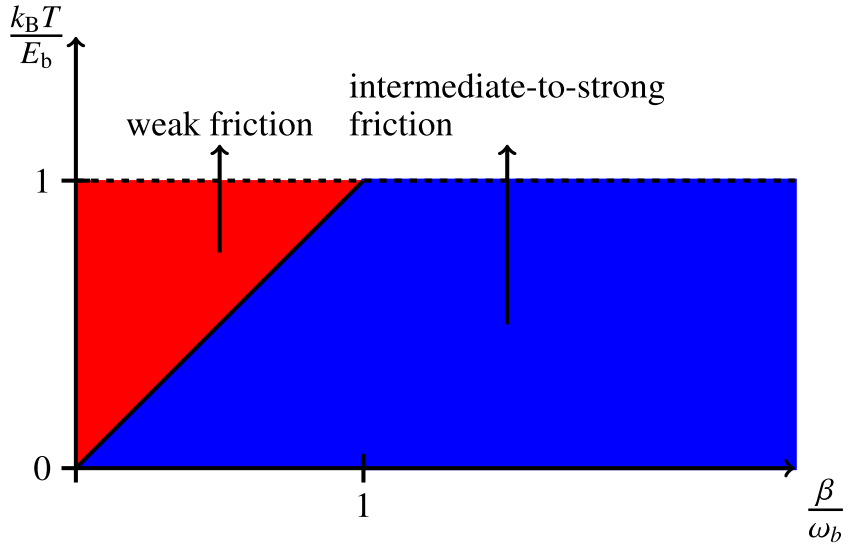

Fig. 4. Classical-rate phase diagram for the two dimensionless parameters $\frac{k_B T}{E_b}$ and $\frac{\beta}{\omega_b}$. The red area denotes the region of weak and the blue area represents the region of intermediate-to-strong friction.
Source: Original figure from [28].

The range of validity of formulas (30), (33) and (35) can be combined into one single diagram, the classical-rate phase diagram, depicting the different regimes as a function of the dimensionless parameters $\frac{k_B T}{E_b}$ and $\frac{\beta}{\omega_b}$ [28] (see Fig. 4). The separating region, also often referred to as turnover region, of weak- and intermediate-to-strong-friction regime can be pointed out by considering condition (31). While the intermediate-to-strong formula (33) is certainly valid for (31), for the limiting case of $k_B T = \beta I(E_b) \approx \beta \frac{E_b}{\omega_a}$ or equivalently for $\frac{k_B T}{E_b} = \frac{\beta}{\omega_a}$, neither (30) nor (33) and (35) are applicable.

Furthermore, given these two formulas it is not difficult to see that both tend to zero in the limits of β going to zero or β going to infinity, respectively. From this, Kramers concluded that the steady-state escape rate must possess a maximum between these two limiting regimes [28,29]. The appearance of the escape rate as a function of β would therefore exhibit a bell-shaped form as depicted in Fig. 5. Ever since Kramers published his paper, researchers in this area tried to find a way to join together the two limiting regimes within one single formula which yields the above-described bell-shaped form [34–37]. A very simple and intuitive approach to give a bridging formula, only using the already known formulas, Eqs. (30) and (33), reads [28]:

$$k_{A\to C} = \left(k^{-1}(\text{low damping}) + k^{-1}(\text{moderate-to-strong damping})\right)^{-1}, \quad \forall \beta \in \mathbb{R}_0^+. \tag{36}$$

Before turning to the extensions of the classical model, special attention has to be given to a term common to Eqs. (30), (33) and (35) for the escape rate in the different limiting regimes. This expression, given by

$$k_{\text{TST}} = \frac{\omega_a}{2\pi} \exp\left[-\frac{E_b}{k_B T}\right], \tag{37}$$

where the subscript, TST, stands for transition-state theory, denotes the escape rate for the TST. The TST-rate is very similar to Kramers' escape rate. The substantial difference between these two rates is, however, that TST assumes that a trajectory overcoming the potential barrier will never return to the initial well [28]. Hence, the TST-rate has to be always an upper bound to Kramers' escape

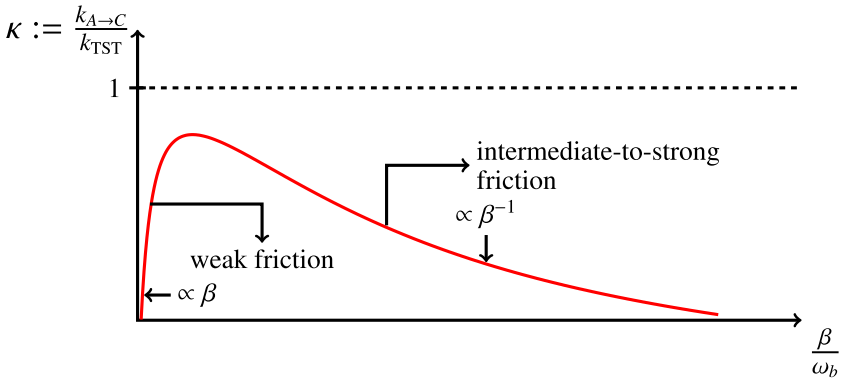

Fig. 5. Schematic representation of the bell-shaped curvature of the steady-state escape rate $k_{A\to C}$, normalized to the transition-state rate k_{TST} (see Eq. (37)), as a function of the dimensionless parameter $\frac{\beta}{\omega_b}$. (For interpretation of the references to color in this figure legend, the reader is referred to the web version of this article.)
Source: Original figure from Ref. [28].

rate [28]. This implies that k_{TST} is an adequate scale to normalize the steady-state escape rate $k_{A\to C}$ (see Fig. 5),

$$k_{A\to C} = \kappa k_{\mathrm{TST}}, \quad \kappa \leq 1. \tag{38}$$

3.2. Extensions of the classical model

Ever since Kramers published his work a great variety of extensions were carried out for his classical model. Among other things Kramers' classical one-dimensional treatment was extended to a multidimensional system for both limiting regimes of the damping rate β [38,39]. Furthermore, corrections of the escape rate in the spatial-diffusion regime arising from anharmonicities of the potential [40–42], the influence of a non-Gaussian white noise [43–45], and quantum effects like quantum tunneling [46,47] were investigated [23].

All these extensions are of Markovian nature, meaning that there is a clear-cut separation between the angular frequency ω_a in the initial potential well and the correlation time τ_{corr} [23], related to the thermal bath, of the form,

$$\tau_{\mathrm{corr}} \ll \frac{2\pi}{\omega_a}. \tag{39}$$

If there exists such a clear separation between the relevant time scales, the classical Markovian LE, Eq. (20), is appropriate to describe the time-evolution of a Brownian particle being subjected to an external potential $V(x)$. However, this might not be the case for various applications [23]. Whenever τ_{corr} is of the order of $2\pi\omega_a^{-1}$ or even larger, the classical escape rates $k_{A\to C}$ for weak and strong friction β (see Eqs. (30), (33), (35)) derived by Kramers are no longer applicable. In this case a non-Markovian treatment of Kramers' escape rate problem is required [23]. In contrast to the classical model (see previous subsection) the Brownian motion in the asymmetric double-well potential (see Fig. 2) is described by the GLE [48], complemented by the external potential field $V(x)$,

$$\begin{aligned} \dot{x} &= v, \\ \dot{v} &= -\frac{1}{m}\frac{dV(x)}{dx} - \frac{1}{m}\int_0^t \Gamma(t-t')v(t')\mathrm{d}t' + \frac{\xi}{m}, \quad \langle \xi(t)\rangle = 0, \end{aligned} \tag{40}$$

whereby it should be recalled that the centered noise $\xi(t)$ and the dissipation kernel $\Gamma(t)$ are related by the second fluctuation–dissipation theorem

$$\Gamma(|t|) = \frac{1}{k_B T} \langle \xi(0)\xi(t) \rangle \,. \tag{41}$$

As a note, Eq. (20) results from Eq. (40) if $\Gamma(t - t') = 2\gamma\delta(t - t')$.

Again, there are two limiting regimes as a function of the damping rate β, the weak- and the strong-friction regime. As in the classical treatment the weak-friction regime is governed by energy diffusion – or equivalently action diffusion – described by [49]

$$\frac{\partial P(I,t)}{\partial t} = \frac{\partial}{\partial I}\left\{ 2\pi\epsilon(I)\left[2\pi k_B T \frac{\partial}{\partial I} + \omega(I) \right] P(I,t) \right\}, \tag{42}$$

where $\omega(I)$ is specified by the potential $V(x)$ and $\epsilon(I)$ is defined as [34,50].

$$\epsilon(I) = \frac{1}{\omega^2(I)} \int_0^\infty \Gamma(t) \langle v(0)v(t) \rangle \, \mathrm{d}t. \tag{43}$$

Hereby, $v(t)$ is to be obtained by solving (40) without dissipation kernel $\Gamma(t)$ and noise $\xi(t)$ [34] for constant energy $E(I)$ and $\langle v(0)v(t) \rangle$ corresponds to the average over the initial phase ϕ_0, where as in Section 3.1 relation (29) applies.

From the diffusion equation for the action, Eq. (42), the mean first passage time $\tau_{\mathrm{MFP}}(I_0, I)$ to reach a final action I, starting from an initial action I_0 can be derived ([49] and references therein),

$$\tau_{\mathrm{MFP}}(I_0, I) = \frac{1}{k_B T} \int_{I_0}^{I} \left\{ \frac{\exp\left[\frac{E(x)}{k_B T}\right]}{\epsilon(x)} \int_0^x \exp\left[-\frac{E(y)}{k_B T} \right] \mathrm{d}y \right\} \mathrm{d}x. \tag{44}$$

The steady-state escape rate $k_{A\to C}$ in the weak-friction regime is then obtained by averaging the mean first passage time $\tau_{\mathrm{MFP}}(I, I_b)$ with regard to the steady-state distribution $P_{\mathrm{SS}}(I)$ inside the initial well [49]

$$k_{A\to C} = \left[\int_0^{I_B} P_{\mathrm{SS}}(I) \tau_{\mathrm{MFP}}(I, I_b) \mathrm{d}I \right]^{-1}. \tag{45}$$

Supposing the well is deep enough, it can be assumed that $P_{\mathrm{SS}}(I)$ is Boltzmann distributed. Inserting the Boltzmann distribution together with Eq. (44) in Eq. (45) a very compact approximate formula for the steady-state escape rate $k_{A\to C}$ in the weak-friction regime is obtained [49]:

$$k_{A\to C} = \frac{\omega_a \epsilon(I_b)\omega(I_b)}{k_B T} \exp\left[-\frac{E_b}{k_B T} \right], \tag{46}$$

where $\epsilon(I_b)$ is to be computed via Eq. (43).

In the intermediate-to-strong-friction regime the corresponding diffusion equation is referred to as generalized Fokker–Planck equation (GFPE) and given by Eq. (87), which will be discussed in detail in Section 3.3. The associated escape rate $k_{A\to C}$ is [23]

$$k_{A\to C} = \frac{\lambda_{\mathrm{NM}}}{\omega_b} \frac{\omega_a}{2\pi} \exp\left[-\frac{E_b}{k_B T} \right], \tag{47}$$

where λ_{NM} is defined as

$$\lambda_{\mathrm{NM}} = \sqrt{\frac{\bar{\beta}^2}{4} + \bar{\omega}^2} - \frac{\bar{\beta}}{2} \tag{48}$$

and the subscript NM represents the non-Markovian case. The meaning of $\bar{\beta}$ and $\bar{\omega}$ and the relation (48) will be specified in Section 3.3. This result for the steady-state escape rate $k_{A\to C}$ in case of a non-Markovian treatment of Kramers' classical escape rate problem is formally identical to the appropriate result for the classical model (see Eq. (33)). One only needs to exchange λ_{M} with λ_{NM} or the bare damping β and frequency ω_b with their non-Markovian analogues $\bar{\beta}$ and $\bar{\omega}$ [23]. For correlation function C_1, Eq. (12), the computation of λ_{NM} is indicated in Appendix B.

3.3. Derivation of Kramers' escape rate in the spatial-diffusion regime (intermediate-to-strong friction)

In this subsection the appropriate quasi-steady-state escape rate $k_{A\to C}$ from the reactant well A to the product well C (see Fig. 2) in the intermediate-to-strong-friction regime, also referred to as spatial-diffusion regime, will be explicitly derived, following what was done in Ref. [28,29] in the Markovian case and Ref. [23] in the non-Markovian case.

For the following considerations it is possible to handle the quasi-steady-state rate as a real steady-state rate without influencing the underlying physics, provided that the condition $E_\mathrm{b} \gg k_\mathrm{B}T$ holds [34]. To that end, the initial A-well is provided with a source, feeding it with particles at energies much smaller than the barrier height E_b and the B-well with a sink, removing particles that traversed the barrier [28,34].

Before starting with the actual derivation, it should be emphasized that the steady-state escape rate in the spatial-diffusion regime is essentially characterized by the dynamics around the top of the barrier at x_b [23]. In both cases the main task will be to determine the stationary probability density $\rho(x, v)$, obeying various boundary conditions – which will be specified later – for the stationary current j. For a given probability density $\rho(x, v)$ it is then easy to compute the population n_a of the Brownian particles in the initial A-Well, given by

$$n_a = \int_{-\infty}^{x_b} \rho(x, v)\mathrm{d}x\mathrm{d}v \tag{49}$$

and the current j_b with respect to the barrier top at $x = x_b$, obtained by

$$j_b = \int_{-\infty}^{\infty} v\rho(x_b, v)\mathrm{d}v. \tag{50}$$

Inserting the appropriate solutions of (49) and (50) into Eq. (23) the steady-state escape rate $k_{A\to C}$ from the A- to the C-well is readily calculated.

Markovian case The Markovian Brownian motion in an external potential field $V(x)$ is described by the LE, Eq. (20). This equation can be transformed into its corresponding FPE, Eq. (32). As already mentioned above, the essential dynamics of the spatial-diffusion regime is restricted to the vicinity of the barrier top. Expanding the potential $V(x)$ around x_b, i.e.

$$V(x) \approx V(x_b) - \frac{1}{2}m\omega_b^2(x - x_b)^2, \quad x \approx x_b, \tag{51}$$

the corresponding FPE reads

$$\left[-v\frac{\partial}{\partial x} - \frac{\partial}{\partial v}\left(-\frac{\gamma}{m}v + \omega_b^2(x - x_b)\right) + \frac{D}{2m^2}\frac{\partial^2}{\partial v^2}\right]\rho(x, v) = 0, \quad x \approx x_b, \tag{52}$$

where the in general dynamic probability density $P(x, v, t)$ is replaced by the stationary probability density $\rho(x, v)$ in search of a stationary escape rate.

To determine a general solution $\rho(x, v)$ for Eq. (52) Kramers then used the ansatz [28,29]

$$\rho(x, v) = \frac{1}{Z}\Xi(x, v)\exp\left[-\frac{\frac{1}{2}mv^2 + V(x)}{k_\mathrm{B}T}\right]. \tag{53}$$

Following what Kramers did, two limiting cases for $\rho(x, v)$, leading to several boundary conditions for $\Xi(x, v)$, have to be considered. Inside the well in a small area around the bottom located at x_a (see Fig. 2) the particles are assumed to be thermalized. This is a reasonable requirement given that $E_\mathrm{b} \gg k_\mathrm{B}T$. Hence, the probability density around $x \approx x_a$ is well approximated by a Boltzmann distribution,

$$\rho(x, v) = \frac{1}{Z}\exp\left[-\frac{\frac{1}{2}mv^2 + V(x)}{k_\mathrm{B}T}\right], \quad x \approx x_a. \tag{54}$$

Comparing both expressions, Eqs. (53) and (54), the first boundary condition for $\Xi(x, v)$ is identified as

$$\Xi(x, v) \approx 1, \quad x \approx x_a. \tag{55}$$

Furthermore, the probability density $\rho(x, v)$ is supposed to vanish beyond the barrier at $x = x_b$, i.e.

$$\rho(x, v) \approx 0, \quad x > x_b, \tag{56}$$

since the particles are removed by a sink leading to

$$\Xi(x, v) \approx 0, \quad x > x_b. \tag{57}$$

For $\Xi(x, v)$ to obey these two limits (Eqs. (55) and (57)) Kramers assumed it to be only dependent on a linear combination of position and velocity [28,29], i.e.

$$\Xi(x, v) = \Xi(z), \quad z = v - b(x - x_b), \tag{58}$$

where b denotes a yet undetermined constant. By inserting the general expression for the probability density $\rho(x, v)$, Eq. (53), into the FPE of $\rho(x, v)$ around x_b, Eq. (52) the appropriate FPE for $\Xi(x, v)$ is obtained:

$$\left[-v\frac{\partial}{\partial x} - \left(\frac{\gamma}{m}v + \omega_b^2(x - x_b)\right)\frac{\partial}{\partial v} + \frac{D}{2m^2}\frac{\partial^2}{\partial v^2}\right]\Xi(x, v) = 0. \tag{59}$$

Using furthermore relation (58) the FPE for $\Xi(x, v)$, Eq. (59), can be converted into the corresponding FPE for $\Xi(z)$,

$$\left[\left(\left(b - \frac{\gamma}{m}\right)v - \omega_b^2(x - x_b)\right)\frac{\partial}{\partial z} + \frac{D}{2m^2}\frac{\partial^2}{\partial z^2}\right]\Xi(z) = 0, \tag{60}$$

where the relations

$$\frac{\partial \Xi}{\partial x} = \frac{\partial \Xi}{\partial z}\underbrace{\frac{\partial z}{\partial x}}_{=-b} = -b\frac{\partial \Xi}{\partial z}, \tag{61}$$

$$\frac{\partial \Xi}{\partial v} = \frac{\partial \Xi}{\partial z}\underbrace{\frac{\partial z}{\partial v}}_{=1} = \frac{\partial \Xi}{\partial z}, \tag{62}$$

$$\frac{\partial^2 \Xi}{\partial v^2} = \frac{\partial}{\partial v}\left(\frac{\partial \Xi}{\partial v}\right) = \frac{\partial}{\partial v}\left(\frac{\partial \Xi}{\partial z}\right) = \frac{\partial}{\partial z}\left(\frac{\partial \Xi}{\partial v}\right) = \frac{\partial}{\partial z}\left(\frac{\partial \Xi}{\partial z}\right) = \frac{\partial^2 \Xi}{\partial z^2} \tag{63}$$

have been applied. To proceed further, by requiring that

$$\left(b - \frac{\gamma}{m}\right)v - \omega_b^2(x - x_b) = \lambda z, \tag{64}$$

Kramers transformed Eq. (59) into the ordinary differential equation

$$\left[\lambda z\frac{\partial}{\partial z} + \frac{D}{2m^2}\frac{\partial^2}{\partial z^2}\right]\Xi(z) = 0, \quad \forall x \approx x_b,\ v. \tag{65}$$

Eqs. (64) and (58) determine the two constants b and λ:

$$\left(b - \frac{\gamma}{m}\right)v - \omega_b^2(x - x_b) = \lambda z = \lambda(v - b(x - x_b)), \tag{66}$$

$$\Rightarrow \left(b - \frac{\gamma}{m}\right)v - \omega_b^2(x - x_b) = \lambda v - \lambda b(x - x_b). \tag{67}$$

Therefore, by comparison of coefficients one finds

$$\lambda = b - \frac{\gamma}{m}, \tag{68}$$

$$\lambda b = \omega_b^2 \tag{69}$$

which leads to a quadratic relation for b by insertion of Eq. (68) into Eq. (69)

$$b^2 - \frac{\gamma}{m}b - \omega_b^2 = 0. \tag{70}$$

Calculating the roots results in

$$b_\pm = \frac{\beta}{2} \pm \sqrt{\left(\frac{\beta}{2}\right)^2 + \omega_b^2}, \tag{71}$$

where $\beta = \frac{\gamma}{m}$. Replacing then b by $b_\pm$ in Eq. (68) $\lambda_\pm$ is obtained by

$$\lambda_\pm = -\frac{\beta}{2} \pm \sqrt{\left(\frac{\beta}{2}\right)^2 + \omega_b^2}. \tag{72}$$

Now that $\lambda_\pm$ are well defined, the next objective is to solve the ordinary differential equation, Eq. (65), for $\Xi(z)$. Using the ansatz

$$\zeta = \frac{\partial \Xi}{\partial z}, \tag{73}$$

differential equation (65) can be transformed into

$$\frac{\partial \zeta}{\partial z} = -\frac{\lambda z}{A}\zeta, \tag{74}$$

where $A = \frac{D}{2m^2}$. By integration of Eq. (74) the solution for ζ is given by

$$\zeta = \zeta_0 \exp\left[-\frac{\lambda z^2}{2A}\right]. \tag{75}$$

To obtain Ξ another integration has to be performed

$$\Xi(z) = \zeta_0 \int_{-\infty}^{z} \exp\left[-\frac{\lambda s^2}{2A}\right] \mathrm{d}s. \tag{76}$$

Due to boundary conditions (55) and (57) the integration of Eq. (76) over all z has to be equal to one which therefore determines the integration constant to be

$$\zeta_0 = \sqrt{\frac{\lambda_+}{2\pi A}}, \tag{77}$$

where λ in Eq. (76) is identified with the positive root λ_+ for the integral to be convergent [28]. Finally, Ξ is given in the following form:

$$\Xi(z) = \sqrt{\frac{\lambda_+}{2\pi A}} \int_{-\infty}^{z} \exp\left[-\frac{\lambda_+ s^2}{2A}\right] \mathrm{d}s. \tag{78}$$

The next objective will be to determine the population of the A-well n_a and the current j_b over the barrier top to subsequently derive Kramers' result for the spatial-diffusion regime. Insertion of the result for Ξ, Eq. (78), in Kramers' ansatz for the probability density $\rho(x, v)$ (53) and expanding the potential $V(x)$ around x_a, i.e.

$$V(x) \approx V(x_a) + \frac{1}{2} m\omega_a^2 (x - x_a)^2, \quad x \approx x_a, \tag{79}$$

n_a is readily obtained calculating (49) using Eqs. (54) and (79):

$$\begin{aligned} n_a &= \int_{-\infty}^{\infty} \rho(x, v) \mathrm{d}x \mathrm{d}v, \quad x \approx x_a \\ &\approx \frac{1}{Z} \frac{k_\mathrm{B} T}{m} \frac{2\pi}{\omega_a} \exp\left[-\frac{V(x_a)}{k_\mathrm{B} T}\right]. \end{aligned} \tag{80}$$

Computation of the integral (50), using the expansion of the potential $V(x)$ around x_b evaluated at x_b, Eq. (51), and Eq. (53), yields

$$\begin{aligned} j_b &= \int_{-\infty}^{\infty} v\rho(x_b, v)\mathrm{d}v \\ &= \frac{1}{Z}\sqrt{\frac{m'}{\pi}}\exp\left[-\frac{V(x_b)}{k_\mathrm{B}T}\right]\frac{\sqrt{\pi}}{2\sqrt{m'}}\underbrace{\int_{-\infty}^{\infty} v\exp\left[-kv^2\right]\mathrm{d}v}_{=0} \\ &+ \frac{1}{Z}\sqrt{\frac{m'}{\pi}}\exp\left[-\frac{V(x_b)}{k_\mathrm{B}T}\right]\frac{\sqrt{\pi}}{2\sqrt{m'}}\underbrace{\int_{-\infty}^{\infty} v\exp\left[-kv^2\right]\mathrm{erf}(v\sqrt{m'})\mathrm{d}v}_{=\frac{\sqrt{m'}}{k\sqrt{k+m'}}} \\ &= \frac{1}{Z}\exp\left[-\frac{V(x_b)}{k_\mathrm{B}T}\right]\frac{\sqrt{m'}}{2k\sqrt{k+m'}}, \end{aligned} \tag{81}$$

where to the third equality sign $k = \frac{m}{2k_\mathrm{B}T}$ and $m' = \frac{\lambda_+}{2A}$ have been substituted. Resubstitution of $A = \frac{D}{2m^2}$ - making use of relation Eq. (21) -, k, and m' in (81) yields

$$j_b = \frac{1}{Z}\frac{k_\mathrm{B}T}{m}\frac{\lambda_+}{\omega_b}\exp\left[-\frac{V(x_b)}{k_\mathrm{B}T}\right]. \tag{82}$$

Finally, Kramers' result for the steady-state escape rate $k_{A\to C}$, indicated in Section 3.1, is obtained by means of Eq. (23), using Eqs. (80) and (82) and defining $\lambda_+ := \lambda_\mathrm{M}$:

$$k_{A\to C} = \frac{\lambda_\mathrm{M}}{\omega_b}\frac{\omega_a}{2\pi}\exp\left[-\frac{E_\mathrm{b}}{k_\mathrm{B}T}\right], \tag{83}$$

where $E_\mathrm{b} = V(x_b) - V(x_a)$.

Non-Markovian case In case of colored noise the non-Markovian Brownian motion around the barrier in an asymmetric double-well potential $V(x)$ can be described by the GLE (40), introducing the new notation $y = x - x_b$:

$$\begin{aligned} \dot{y} &= \dot{x} = v, \\ \dot{v} &= \omega_b^2 y - \frac{1}{m}\int_0^t \Gamma(t-t')v(t')\mathrm{d}t' + \frac{\xi(t)}{m}, \end{aligned} \tag{84}$$

where $V(x)$ is expanded around x_b yielding

$$V(y) = V(x_b) - \frac{1}{2}m\omega_b^2 y^2, \tag{85}$$

and $\xi(t)$ is a centered stationary Gaussian process

$$\langle\xi(t)\rangle = 0, \tag{86}$$

obeying the second fluctuation–dissipation theorem (see Eq. (41)). The corresponding GFPE around $x \approx x_b$ for the probability density $P(x, v, t)$ of the system, described by (84), is given by [23,51]

$$\begin{aligned} \frac{\partial P(x,v,t)}{\partial t} &= \left[-v\frac{\partial}{\partial y} - \frac{\partial}{\partial v}\left(-\bar{\beta}(t)v + \bar{\omega}_b^2(t)y\right) + \bar{\beta}(t)\frac{k_\mathrm{B}T}{m}\frac{\partial^2}{\partial v^2}\right]P(x,v,t) \\ &+ \frac{k_\mathrm{B}T}{m\omega_b^2}\left(\bar{\omega}_b^2(t) - \omega_b^2\right)\frac{\partial^2 P(x,v,t)}{\partial v\partial y} \end{aligned} \tag{87}$$

with

$$\bar{\beta}(t) = -\frac{\dot{a}(t)}{a(t)}, \tag{88}$$

$$\bar{\omega}_b^2(t) = -\frac{b(t)}{a(t)}, \tag{89}$$

where

$$a(t) = \chi_y(t)\dot{\chi}_v(t) - \dot{\chi}_y(t)\chi_v(t), \tag{90}$$

$$b(t) = \dot{\chi}_y(t)\ddot{\chi}_v(t) - \ddot{\chi}_y(t)\dot{\chi}_v(t), \tag{91}$$

and

$$\chi_y(t) = 1 + \omega_b^2 \int_0^t \chi_v(\tau)\mathrm{d}\tau. \tag{92}$$

In the latter equation $\chi_v(t)$ is given by the inverse Laplace transform (LT)

$$\chi_v(t) = \mathcal{L}^{-1}\left[\frac{1}{s^2 - \omega_b^2 + \frac{\tilde{\Gamma}}{m}s}\right], \tag{93}$$

where $\tilde{\Gamma}(s)$ is the LT of the dissipation kernel $\Gamma(t)$. For a detailed derivation reference is made to Ref. [51]. Nonetheless, a brief motivation and explanation of distinct terms of the above GFPE shall be given next. Comparing the classical FPE and the GFPE (Eqs. (32) and (87)) several similarities are remarkable. Except for an additional diffusive term the GFPE corresponds to the classical FPE, where the damping rate β and the frequency ω_b are replaced by a time dependent damping rate $\bar{\beta}(t)$ and a time dependent frequency $\bar{\omega}_b(t)$. Furthermore, both functions depend on the frequency ω_b and the dissipation kernel $\Gamma(t)$ [51]. In the Markovian limit, where $\Gamma(t) = 2\gamma\delta(t)$, $\bar{\beta}(t) = \beta$, and $\bar{\omega}_b(t) = \omega_b$, the classical FPE is obtained.

The next step is to show where relation (92) is derived from. Given the GLE (84) and performing its Laplace transform one obtains (using Eqs. (A.7), (A.8), (A.9))

$$s\tilde{Y} - y_0 = \tilde{V}, \tag{94}$$

$$s\tilde{V} - v_0 = \omega_b^2\tilde{Y} - \frac{\tilde{\Gamma}}{m}\tilde{V} + \frac{\tilde{\Xi}}{m}, \tag{95}$$

where capital letters with tilde denote the Laplace transforms of the corresponding quantities. Inserting the first relation, Eq. (94), into the second one, Eq. (95), and subsequently solving the resulting expression for $\tilde{Y}$ yields

$$s\left(s\tilde{Y} - y_0\right) - v_0 = \omega_b^2\tilde{Y} - \frac{\tilde{\Gamma}}{m}\left(s\tilde{Y} - y_0\right) + \frac{\tilde{\Xi}}{m}, \tag{96}$$

$$\Rightarrow \tilde{Y} = \frac{y_0\left(s + \frac{\tilde{\Gamma}}{m}\right) + v_0 + \frac{\tilde{\Xi}}{m}}{s^2 - \omega_b^2 + \frac{\tilde{\Gamma}}{m}s}. \tag{97}$$

The inverse Laplace transform of Eq. (97) then leads to [51]

$$y(t) = y_0\chi_y(t) + v_0\chi_v(t) + \frac{1}{m}\int_0^t \chi_v(t - t')\xi(t')\mathrm{d}t', \tag{98}$$

where $\chi_y(t)$ and $\chi_v(t)$ are defined by

$$\chi_y(t) = \mathcal{L}^{-1}\left[\frac{\left(s + \frac{\tilde{\Gamma}}{m}\right)}{s^2 - \omega_b^2 + \frac{\tilde{\Gamma}}{m}s}\right] = \frac{\langle y(t)y_0\rangle}{\langle y_0^2\rangle}, \tag{99}$$

$$\chi_v(t) = \mathcal{L}^{-1}\left[\frac{1}{s^2 - \omega_b^2 + \frac{\tilde{\Gamma}}{m}s}\right] = \frac{\langle y(t)v_0\rangle}{\langle v_0^2\rangle} = \frac{m}{k_\mathrm{B}T}\langle y(t)v_0\rangle. \tag{100}$$

By an analogous procedure the solution for $v(t)$ can be determined [51]

$$v(t) = y_0\dot{\chi}_y(t) + v_0\dot{\chi}_v(t) + \frac{1}{m}\int_0^t \dot{\chi}_v(t - t')\xi(t')\mathrm{d}t', \tag{101}$$

where $\dot{\chi}_y(t)$ is given by

$$\dot{\chi}_y(t) = \omega_b^2 \mathcal{L}^{-1}\left[\frac{1}{s^2 - \omega_b^2 + \frac{\bar{\Gamma}}{m}s}\right] \tag{102}$$

and $\dot{\chi}_v(t)$ is defined as

$$\dot{\chi}_v(t) = \mathcal{L}^{-1}\left[\frac{s}{s^2 - \omega_b^2 + \frac{\bar{\Gamma}}{m}s}\right]. \tag{103}$$

Comparing Eqs. (100) and (102) the above connection between $\chi_y(t)$ and $\chi_v(t)$ (see Eq. (92)) is obtained,

$$\dot{\chi}_y(t) = \omega_b^2 \chi_v(t) \;\Rightarrow\; \chi_y(t) = 1 + \omega_b^2 \int_0^t \chi_v(\tau)\mathrm{d}\tau, \tag{104}$$

where the relation $\chi_y(0) = 1$ has been employed, which follows from Eq. (99).

Turning now again to the actual task of this section, namely the derivation of the steady-state escape rate, the first objective will be to determine the stationary probability density $\rho(x, v)$. As in the original derivation Kramers' ansatz

$$\rho(x, v) = \frac{1}{Z}\Xi(x, v)\exp\left[-\frac{\frac{mv^2}{2} + V(x)}{k_\mathrm{B}T}\right] \tag{105}$$

is used, where the same boundary conditions apply (see Eqs. (55) and (57)). Inserting Eq. (105) into the GFPE (87), the corresponding GFPE for Ξ is obtained,

$$\begin{aligned} v\frac{\partial \Xi}{\partial y} + \bar{\omega}_b^2 y\frac{\partial \Xi}{\partial v} =& \frac{k_\mathrm{B}T}{m}\bar{\beta}\frac{\partial^2 \Xi}{\partial v^2} - \bar{\beta}v\frac{\partial \Xi}{\partial v} \\ &+ \frac{k_\mathrm{B}T}{m\omega_b^2}\left(\bar{\omega}_b^2 - \omega_b^2\right)\left[\frac{m\omega_b^2 y}{k_\mathrm{B}T}\frac{\partial \Xi}{\partial v} - \frac{mv}{k_\mathrm{B}T}\frac{\partial \Xi}{\partial y} + \frac{\partial^2 \Xi}{\partial y \partial v}\right], \end{aligned} \tag{106}$$

whereby the time dependent functions $\bar{\beta}(t)$ and $\bar{\omega}_b^2(t)$ from Eq. (87) have been substituted by the stationary quantities $\bar{\beta}$ and $\bar{\omega}_b^2$, defined by

$$\bar{\beta} = \lim_{t\to\infty}\bar{\beta}(t), \quad \bar{\omega}_b^2 = \lim_{t\to\infty}\bar{\omega}_b^2(t). \tag{107}$$

Again, $\Xi(y, v)$ is demanded to depend on a linear combination of y and v,

$$\Xi(y, v) = \Xi(z), \quad z = v - by, \tag{108}$$

where b is again a yet undetermined constant. With

$$\frac{\partial \Xi(z)}{\partial v} = \frac{\partial \Xi}{\partial z}\frac{\partial z}{\partial v} = \frac{\partial \Xi}{\partial z}, \tag{109}$$

$$\frac{\partial \Xi(z)}{\partial y} = \frac{\partial \Xi}{\partial z}\frac{\partial z}{\partial y} = -b\frac{\partial \Xi}{\partial z}, \tag{110}$$

$$\frac{\partial^2 \Xi(z)}{\partial v^2} = \frac{\partial}{\partial v}\left(\frac{\partial \Xi}{\partial z}\right) = \frac{\partial}{\partial z}\left(\frac{\partial \Xi(z)}{\partial v}\right) = \frac{\partial}{\partial z}\left(\frac{\partial \Xi}{\partial z}\right) = \frac{\partial^2 \Xi}{\partial z^2}, \tag{111}$$

$$\frac{\partial^2 \Xi(z)}{\partial y \partial v} = \frac{\partial}{\partial y}\left(\frac{\partial \Xi}{\partial z}\frac{\partial z}{\partial v}\right) = \frac{\partial}{\partial z}\left(\frac{\partial \Xi}{\partial y}\right) = \frac{\partial}{\partial z}\left(-b\frac{\partial \Xi}{\partial z}\right) = -b\frac{\partial^2 \Xi}{\partial z^2} \tag{112}$$

the GFPE for $\Xi(z)$ is given by

$$\begin{aligned} \left(-vb + \bar{\omega}_b^2 y\right)\frac{\partial \Xi}{\partial z} =& \frac{k_\mathrm{B}T}{m}\bar{\beta}\frac{\partial^2 \Xi(z)}{\partial z^2} - \bar{\beta}v\frac{\partial \Xi}{\partial z} + \frac{k_\mathrm{B}T}{m\omega_b^2}\left(\bar{\omega}_b^2 - \omega_b^2\right)\frac{m\omega_b^2 y}{k_\mathrm{B}T}\frac{\partial \Xi}{\partial z} \\ &+ \frac{k_\mathrm{B}T}{m}c\left[\frac{mv}{k_\mathrm{B}T}b\frac{\partial \Xi}{\partial z} - b\frac{\partial^2 \Xi}{\partial z^2}\right], \end{aligned} \tag{113}$$

where $c = \frac{\bar{\omega}_b^2 - \omega_b^2}{\omega_b^2}$. Rearranging the terms provides

$$-\left[b(1+c)-\bar{\beta}\right] v \frac{\partial \Xi}{\partial z} + \omega_b^2 y \frac{\partial \Xi}{\partial z} = \frac{k_\mathrm{B}T}{m}\left[\bar{\beta} - cb\right] \frac{\partial^2 \Xi}{\partial z^2}. \tag{114}$$

The next task will be to transform Eq. (114) into an ordinary differential equation by demanding

$$\left[b(1+c)-\bar{\beta}\right] v - \omega_b^2 y = \lambda z = \lambda(v - by). \tag{115}$$

By comparison of coefficients the two following relations are obtained:

$$b(1+c) - \bar{\beta} = \lambda, \tag{116}$$

$$\omega_b^2 = b\lambda \Rightarrow \lambda = \frac{\omega_b^2}{b}. \tag{117}$$

Inserting Eq. (116) into Eq. (117) results in a quadratic relation for b,

$$b(1+c) - \bar{\beta} = \frac{\omega_b^2}{b} \Rightarrow b = \frac{\omega_b^2}{b(1+c) - \bar{\beta}}. \tag{118}$$

Computing the roots of the quadratic Eq. (118) using that

$$1 + c = 1 + \frac{\bar{\omega}_b^2 - \omega_b^2}{\omega_b^2} = \frac{\bar{\omega}_b^2}{\omega_b^2}, \tag{119}$$

results in

$$b_\pm = \frac{\omega_b^2}{\bar{\omega}_b^2}\left(\frac{\bar{\beta}}{2} \pm \sqrt{\frac{\bar{\beta}^2}{4} + \bar{\omega}_b^2}\right) \tag{120}$$

or equivalently in

$$\lambda_\pm = -\frac{\bar{\beta}}{2} \pm \sqrt{\frac{\bar{\beta}^2}{4} + \bar{\omega}_b^2} \tag{121}$$

by inserting Eq. (120) into Eq. (117). Solving now the resulting ordinary differential equation, which is formally identical to Eq. (74) in the Markovian case, using boundary conditions (55) and (57), $\Xi(z)$ is given by

$$\Xi(z) = \sqrt{\frac{\lambda_+}{2\pi A}} \int_{-\infty}^{z} \exp\left[-\frac{\lambda_+ s^2}{2A}\right] \mathrm{d}s, \tag{122}$$

where

$$A = \frac{k_\mathrm{B}T\left(\bar{\beta} - b_+ c\right)}{m}, \tag{123}$$

and λ_+ denotes the positive root of Eq. (118) which needs to be employed for the integral term to be convergent. As soon as $\Xi(z)$ and therefore $\rho(z)$ is known, the population n_a in the A-well and the stationary current over the potential barrier j_b can be computed. Calculating the integral for n_a in the non-Markovian case yields the same result as in the Markovian case (see Eq. (80)), since the stationary probability density $\rho(z)$ around x_a is identical. In a region around the top of the barrier at $x = x_b$, however, the density $\rho(z)$ is significantly different from its Markovian analog. Nonetheless even for the computation of j_b the results from the Markovian treatment can be used. Only the quantity m' needs to be replaced by n defined by

$$n = \frac{m(b_+(1+c) - \bar{\beta})}{2k_\mathrm{B}T(\bar{\beta} - b_+ c)}. \tag{124}$$

As in the Markovian case a temporary result is obtained by

$$j_b = \frac{1}{Z}\exp\left[-\frac{V(x_b)}{k_\mathrm{B}T}\right]\frac{\sqrt{n}}{2k\sqrt{k+n}}. \tag{125}$$

Reinserting relation (124) into the temporary result for j_b, Eq. (125), yields

$$j_b = \frac{1}{Z}\frac{k_\mathrm{B}T}{m}\frac{\lambda_+}{\omega_b}\exp\left[-\frac{V(x_b)}{k_\mathrm{B}T}\right]. \tag{126}$$

Finally using Eq. (23) together with (80) and (126) the steady-state escape rate $k_{A\to C}$ is given by

$$k_{A\to C} = \frac{\lambda_\mathrm{NM}}{\omega_b}\frac{\omega_a}{2\pi}\exp\left[-\frac{E_\mathrm{b}}{k_\mathrm{B}T}\right], \tag{127}$$

where again $E_\mathrm{b} = V(x_b) - V(x_a)$ and λ_+ was identified with λ_NM (see Eq. (48)). That is the desired result for $k_{A\to C}$ as indicated in Section 3.2.

Subsequently there are a number of comments to be made about the just derived escape rate $k_{A\to C}$. It can be shown that the prefactor λ_NM of Eq. (127) corresponds to the largest positive root of $s^2 - \omega_b^2 + \frac{\tilde{\Gamma}}{m}s$ [24,34], originating from the inverse Laplace transform $\chi_v(t)$ (see Eq. (100)). For a derivation of this statement reference is made to Ref. [34]. The entire information about the dissipation kernel $\Gamma(t)$ is therefore completely contained in λ_NM. In Appendix B it is shown how to derive λ_NM for correlation function C_1, Eq. (12). For this correlation function the above expression, $s^2 - \omega_b^2 + \frac{\tilde{\Gamma}}{m}s$, becomes a cubic function of s. Thus, in order to compute λ_NM only the cubic roots are needed.

4. Numerical studies

This section is devoted to the core of this work: Kramers' escape rate problem, which was presented in the previous two sections, will be numerically investigated for both white and colored thermal noise. To that end, the colored noise is generated by means of the numerical implementation of the algorithm, indicated in Section 2, which is given in the Appendix of Ref. [31] and the GLE, Eq. (40), is solved using the explicit three-step Adams–Bashforth algorithm [52]:

$$y_0 = a_0, \quad y_1 = a_1, \quad y_2 = a_2, \tag{128}$$

$$y_{i+1} = y_i + \frac{h}{12}\left[23f(t_i, y_i) - 16f(t_{i-1}, y_{i-1}) + 5f(t_{i-2}, y_{i-2})\right], \tag{129}$$

where $i = 2, 3, \ldots, N-1$ and the local and global error are $\mathcal{O}(h^4)$ and $\mathcal{O}(h^3)$, respectively. Furthermore, y stands representative for position and velocity in the GLE, $f(t, y)$ corresponds to its right-hand side, respectively, and h is the step-size. The three values y_0, y_1 and y_2, where y_0 corresponds to the initial conditions and y_1 and y_2 are to be evaluated using Euler's method, are required to apply the above indicated three-step Adams–Bashforth method.

In what follows, a first step will be to present the details of the numerical simulations regarding the used potential $V(x)$, correlation functions, initial conditions, and the algorithm which is employed to compute the escape rate . Afterwards, it will be illustratively shown that the numerical simulations are able to fit the approximate analytic formulas properly to validate the numerical algorithm. For that purpose, the numerical parameters have been adjusted in a region where the approximate formulas are accurate.

Subsequently, Kramers' steady-state escape rate as a function of the friction rate β will be investigated for different correlation functions and compared to the appropriate analytic formulas.

4.1. Numerical setup

In contrast to Kramers' classical model, for the numerical simulations a slightly idealized potential will be used. This potential (see Fig. 6) is composed of two parabolic potentials of the

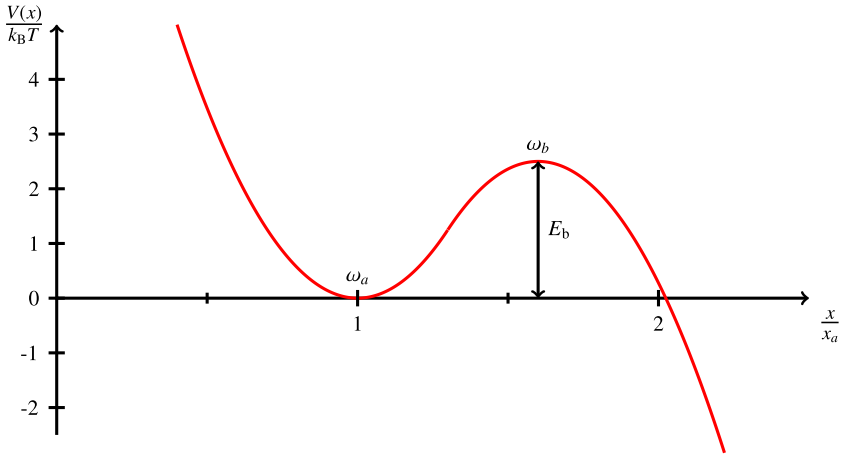

Fig. 6. Potential $V(x)$, Eq. (130), used for the following numerical simulations. Here $m = 1.11\,\text{GeV}$, $T = 1\,\text{GeV}$, $\omega = 5\,\text{GeV}$, $E_b = 2.5\,\text{GeV}$, $x_a = 1\,\text{GeV}^{-1}$, and $x_b = 1.6x_a$.

same frequency $\omega_a = \omega_b = \omega$, smoothly connected at some intermediate point x_m,

$$V(x) = \begin{cases} \frac{m\omega_a^2}{2}(x - x_a)^2 & \text{for} \quad x < x_m, \\ E_b - \frac{m\omega_b^2}{2}(x - x_b)^2 & \text{for} \quad x > x_m, \end{cases} \tag{130}$$

where x_m is defined as

$$x_m = \frac{x_b + x_a}{2}. \tag{131}$$

This idealized potential is to be understood as an asymmetric double-well potential, whereby the right potential well is supposed to be infinitely deep. In doing so, anharmonic corrections [40–42], naturally arising from more realistic potentials, can be largely neglected.

As indicated before, the simulations are performed for white and colored noise, which are connected to an appropriate correlation function, respectively (see Section 2). For the studies of this work the usual correlation function for white noise will be used:

$$C_0 := \langle \xi(t)\xi(0)\rangle = D\delta(t). \tag{132}$$

In addition to that, for colored noise, the three correlation functions C_1, C_2 and C_3 (see Section 2) are covered:

$$C_1(|t|) = \frac{D}{2\tau} \exp\left[-\frac{|t|}{\tau}\right], \tag{133}$$

$$C_2(|t|) = \frac{D}{a\sqrt{\pi}} \exp\left[-\left(\frac{|t|}{a}\right)^2\right], \tag{134}$$

$$C_3(|t|) = \frac{g}{4} k_B T \alpha^2 \left(1 - \frac{\alpha}{\sqrt{m}}|t|\right) \exp\left[-\frac{\alpha}{\sqrt{m}}|t|\right]. \tag{135}$$

By use of the algorithm, described in Section 2, a sequence of the respective colored noise can be generated from the above given correlation functions.

4.2. Simulations

The starting situation of the simulations is as follows: In each simulation, computing the evolution of a whole ensemble, consisting of a large number of about 10^6 realizations of the

stochastic processes $x(t)$ and $v(t)$, respectively, the particles are initialized at the bottom of the left well at $x_0 = x_a$ with velocity $v_0 = 0$. The remaining relevant parameters are given as follows:

$$E_\mathrm{b} = 2.5\,\mathrm{GeV},\ \omega_b = 5\,\mathrm{GeV},\ m = 1.11\,\mathrm{GeV},\ T = 1\,\mathrm{GeV},\ \tau_{corr} = \{0.2,\ 0.4,\ 1\}\,\mathrm{GeV}^{-1}, \quad (136)$$

where different correlation times τ_corr are employed for the non-Markovian correlation functions, Eqs. (133), (134) and (135), as also effects of growing correlation times shall be investigated in the following sections. The choice of magnitude of τ_{corr} is justified due to condition (39), according to which a non-Markovian description requires $\tau_\mathrm{corr} \approx 1\,\mathrm{GeV}^{-1}$ for the above parameters:

$$\tau_\mathrm{corr} = \frac{2\pi}{\omega} \approx 1\,\mathrm{GeV}^{-1}. \quad (137)$$

Vividly speaking, expression (137) implies that there is the fifth part of an oscillation in about $0.2\,\mathrm{GeV}^{-1}$ up to about one oscillation in $1\,\mathrm{GeV}^{-1}$. Hence, the three cases for τ_corr are representative for medium ($\tau_{corr} = 0.2\,\mathrm{GeV}^{-1}$ and $\tau_{corr} = 0.4\,\mathrm{GeV}^{-1}$) and strong ($\tau_{corr} = 1\,\mathrm{GeV}^{-1}$) non-Markovian situations.

Concerning the parameters (136) the attentive reader will immediately notice that $m \approx T$, which implies relativistic velocities[1] by virtue of the equipartition theorem. However, since the Brownian particles used in these simulations are not "aware" of relativity - as they are governed by classical Newtonian dynamics (see Eqs. (20) and (40))- the size of the velocity has no relevance. A relativistic treatment of non-Markovian Brownian motion is left for future work; for the Markovian case, see [16].

Given the solutions for $x(t)$ and $v(t)$ for every realization of the simulation the rate of particles overcoming the potential barrier is readily obtained.

There are two possible ways to numerically determine the steady-state rate. Both include a certain absorptive barrier x_abs which coincides with the sink described in Section 3.3. This absorptive barrier has to be chosen far away from the top of the potential barrier in the right potential well to ensure that particles that have reached the absorptive barrier will never return to the initial well. The two ways of numerical determination of the steady-state current now depend on what happens after reaching this absorptive barrier.

The first method, usually referred to as flux-over-population method [28], is based on the re-initialization of particles which have overcome the absorptive barrier. This leads to a nearly constant population in the initial well. Thereby, it needs to be ensured that these re-initializations are not taken into account as real backscattering which would affect the current over the barrier. The steady-state escape rate is then obtained determining the current over the barrier located at x_b.

The second method on the other hand gets along without any re-initialization. Here, the current is calculated concerning the absorptive barrier. Numerically, the steady-state escape rate is computed as follows [53]:

$$k_{A\to C} = \frac{1}{N_\mathrm{tot} - N_\mathrm{abs}} \frac{\Delta N_\mathrm{abs}}{\Delta t}, \quad (138)$$

where N_tot denotes the total number of initialized particles, N_abs is the total number of particles that have already reached the absorptive border, and ΔN_abs designates the number of particles being absorbed in the course of the time interval Δt. It turns out that both methods yield the same results. The second method, however, seems to be numerically more stable as the first method requires smaller time steps Δt for the escape rate to be convergent. Hence, for the following numerical discussion the second method will be used.

Fig. 7 indicates the typical outcomes of two non-Markovian simulations (correlation function C_1, Eq. (12)) for different correlation times, applying the second numerical method. Basically, the escape rate as a function of time consists of three successive stages. After an initial phase of a not quantifiable escape rate, during which the considered ensemble thermalizes, a transient

[1] The numerical parameters have been adjusted such that the approximate analytical formulas become very accurate to test and validate the numerical method. Though the situation should be treated relativistically from a physical point of view, this does not invalidate the numerical test of the non-relativistic Langevin simulation.

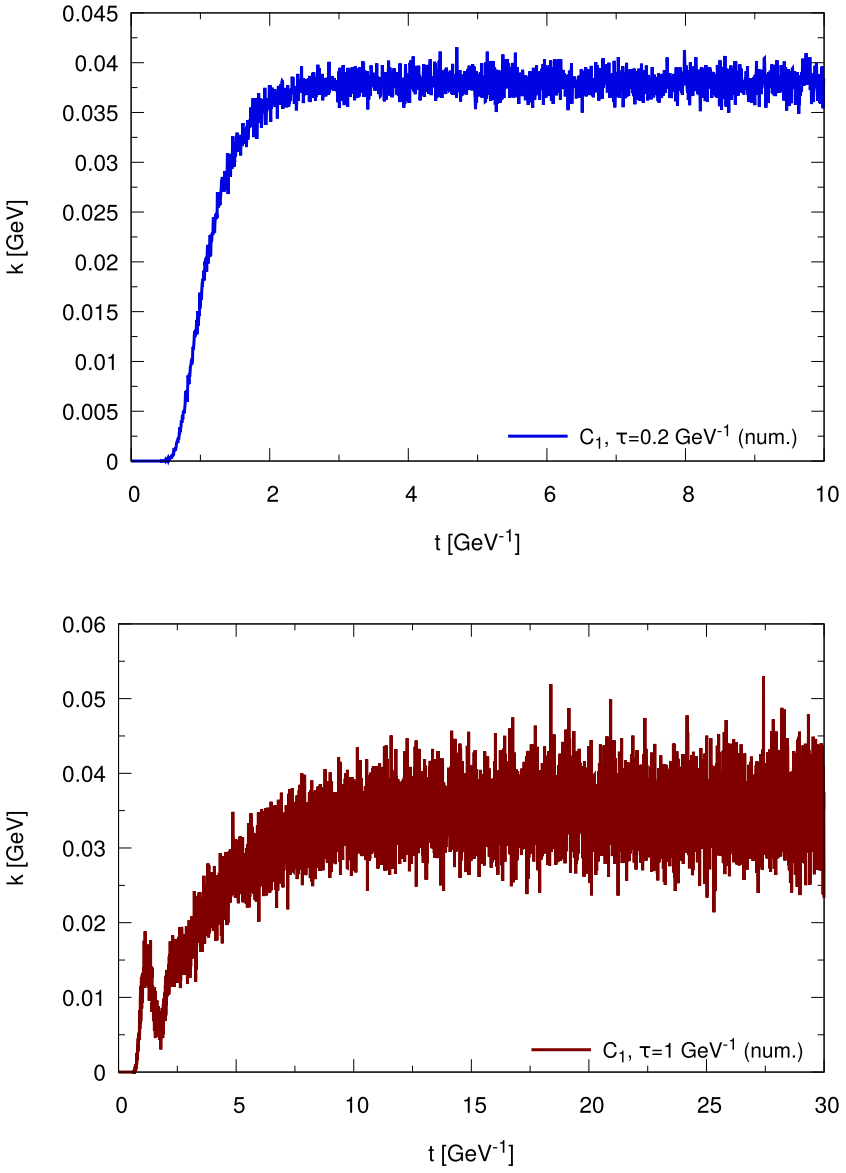

Fig. 7. Escape rate k as a function of time for correlation function C_1, Eq. (12), averaged over $8 \cdot 10^6$ realizations, where $m = 1.11\,\text{GeV}$, $\beta = 9\,\text{GeV}$, $E_\text{b} = 2.5\,\text{GeV}$, $T = 1\,\text{GeV}$, and $\omega = 5\,\text{GeV}$.

phase occurs. In this regime the escape rate begins to rise moderately until in the end it takes a constant mean value, Kramers' steady-state escape rate. In case of the non-Markovian noise and large correlation times (i.e. $\tau \gg \frac{2\pi}{\omega}$) a special feature occurs in the transient phase. After an initial rise, the current significantly decreases until it eventually starts to rise again and finally converges to its mean value (see Fig. 7). This effective backscattering in the transient phase is an example for the memory effects, arising from finite correlation times [31]. The mean value of Kramers' escape rate is evaluated by averaging over the quasi-stationary third stage. Dividing the evolution of rate

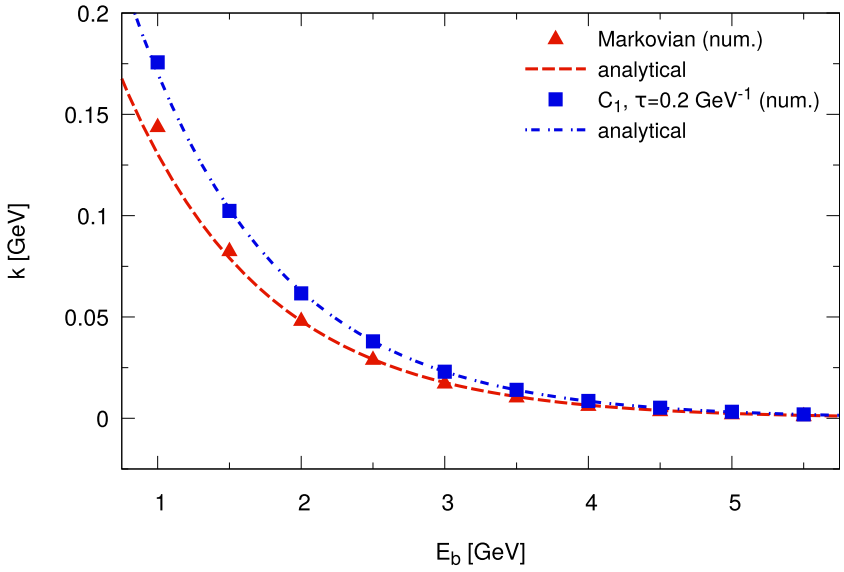

Fig. 8. Steady-state escape rate k as a function of the barrier height E_b, where $\beta = 9\,\mathrm{GeV}$, $\omega_b = 5\,\mathrm{GeV}$, and $T = 1\,\mathrm{GeV}$. Red: Markovian simulations, Eq. (132) (triangles), and analytical solution, computed with Eq. (33) (dashed line). Blue: Non-Markovian simulations for correlation function C_1, Eq. (12), with $\tau = 0.2\,\mathrm{GeV}^{-1}$ (squares) and analytical solution, computed with Eq. (47) with λ_NM given in Appendix B (dotted dashed line).

k into n bins of width Δt and taking only into account the last m steps of the third stage, Kramers' escape rate and the corresponding standard error are evaluated, using the following equations [53]:

$$k_{A\to C} = \frac{1}{m}\sum_{i=n-m}^{n} k_{A\to C}(t_i), \tag{139}$$

$$\sigma_k = \sqrt{\frac{1}{m(m-1)}\sum_{i=n-m}^{n}(k_{A\to C}(t_i) - k_{A\to C})^2}. \tag{140}$$

4.3. Parametrical dependencies

In order to show that the used code and the algorithm to generate colored noise, contained therein, actually work properly, it is useful to numerically examine the occurring parametrical dependencies related to the steady-state escape rate for the δ-correlated Markovian correlation function C_0 and the non-Markovian correlation function C_1 and compare them to the approximate analytical results.

For this purpose the further procedure will be the following: While one parameter is varied, all remaining parameters will be kept constant to see if the isolated parameters obey the correct scaling behavior. The parameters to be studied are the temperature T, the barrier height E_b, and the frequency ω_b. The dependence on the coupling constant β will be investigated separately later on.

Illustratively in what follows a comparison of numerical with analytical results, Eqs. (33) and (47) with λ_NM given in Appendix B, for the above-named parameters will be presented to justify the validity of the underlying numerical algorithm. It should be recalled that λ_NM from Eq. (47) is to be identified with the largest positive root of $s^2 - \omega_b^2 + \frac{\tilde{\Gamma}}{m}s$. As can be seen in Figs. 8–10 the expected analytical behavior (see Eqs. (33) and (47)) could be recovered almost perfectly in each case. Only for small barrier heights E_b compared to the temperature T a deviation from the analytical

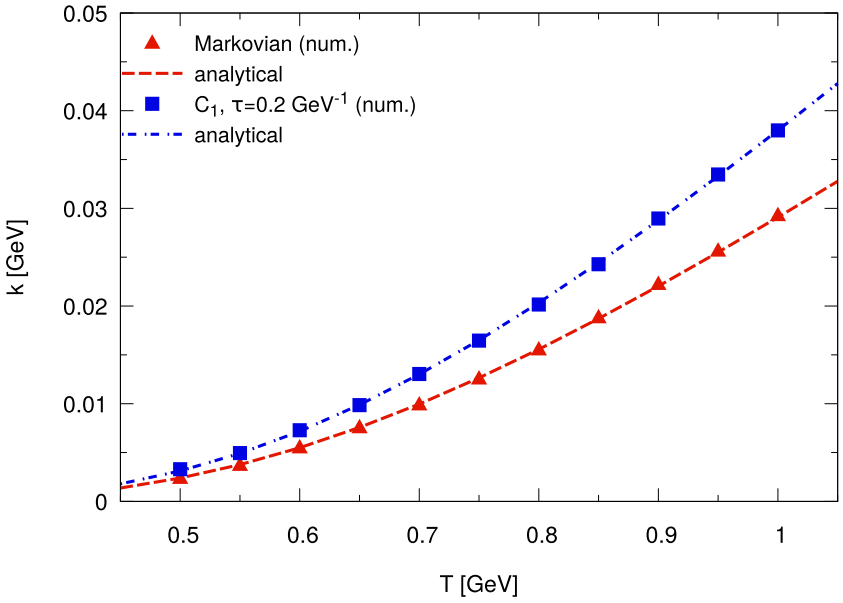

Fig. 9. Steady-state escape rate k as a function of the temperature T, where $\beta = 9\,\text{GeV}$, $\omega_b = 5\,\text{GeV}$, and $E_\text{b} = 2.5\,\text{GeV}$. Red: Markovian simulations, Eq. (132) (triangles), and analytical solution, computed with Eq. (33) (dashed line). Blue: Non-Markovian simulations for correlation function C_1, Eq. (12), with $\tau = 0.2\,\text{GeV}^{-1}$ (squares) and analytical solution, computed with Eq. (47) with λ_NM given in Appendix B (dotted dashed line).

results is visible in Fig. 8. However, this deviation is expected as with decreasing barrier height E_b and simultaneous constant temperature T the approximative analytic formulas, Eqs. (33) and (47) start to lose their validity due to the violation of condition (22). Certainly, this deviation would also eventually appear in Fig. 9 for higher temperatures T.

4.4. Steady-state rate as a function of the damping rate β

In the present section it will be investigated how Kramers' escape rate behaves as a function of the coupling strength or damping rate β for correlation functions C_0, C_1 and C_2, Eqs. (132), (12) and (13) (see also Ref. [34]), and as a function of the dimensionless coupling strength g in case of correlation function C_3, Eq. (14). Since in this context the coupling strengths β or g are the only varying quantities, it is sufficient to restrict the investigation of the Kramers' rate to the coefficient κ of Eq. (38) as it is solely responsible for differences in the behavior of the escape rates regarding different correlation functions. To that end, all rates will be normalized to the transition-state rate k_TST, which is always an upper border to Kramers' escape rate $k_{A\to C}$ as already mentioned in Section 3.1 (see Fig. 5). Doing this in case of white noise, it turns out that κ is a function of the dimensionless parameter $\frac{\beta}{\omega}$ in the weak-friction and of $(\frac{\beta}{\omega})^{-1}$ in the strong-friction regime (see Fig. 5), which as already discussed in Section 3.1 also comes into play concerning the range of validity of the different regimes (see Fig. 4). This will become important for the comparison of numerical and analytical results.

The main objective will be to find out about the peculiarities of a non-Markovian compared to a Markovian correlation function in case of correlation functions C_1 and C_2. Not only the differences between distinct correlation functions but also the differences, relating to changes in the correlation time will be of interest. Therefore, Kramers' escape rate is computed for every correlation function and varying correlation times τ_corr ($0.2\,\text{GeV}^{-1}$, $0.4\,\text{GeV}^{-1}$, and $1\,\text{GeV}^{-1}$) within a fixed area of β-values, covering the small- and the strong-friction regime (see also Fig. 4).

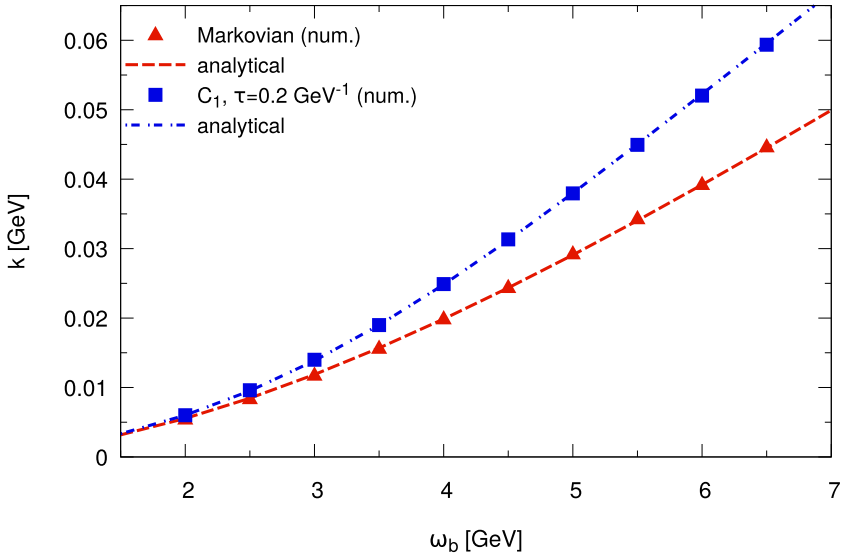

Fig. 10. Steady-state escape rate k as a function of the frequency ω_b, where $\beta = 9\,\mathrm{GeV}$, $T = 1\,\mathrm{GeV}$, and $E_b = 2.5\,\mathrm{GeV}$. Red: Markovian simulations, Eq. (132) (triangles), and analytical solution, computed with Eq. (33) (dashed line). Blue: Non-Markovian simulations for correlation function C_1, Eq. (12), with $\tau = 0.2\,\mathrm{GeV}^{-1}$ (squares) and analytical solution, computed with Eq. (47) with λ_{NM} given in Appendix B (dotted dashed line).

In what follows, one after the other the correlation functions C_1 and C_2 are compared to the Markovian case, starting with correlation function C_1. For correlation function C_3, however, a comparison with the Markovian case will be omitted since no strict Markovian limit exists (see also Section 4.4.3).

It should be noted that when talking about weak and strong friction this is always meant in relation to the friction value, corresponding to the maximal escape rate. This should not be confused with the weak- and strong-friction regimes of Kramers' escape rate problem as these regimes do not only depend on the actual friction value but also on the validity of certain conditions (see also Section 3.1).

4.4.1. Correlation function C_1

First of all, it should be recognized that the steady-state escape rate as a function of the coupling strength β follows the bell-shaped course, already estimated by Kramers [28,29], in both the Markovian and non-Markovian case (see Fig. 11). In the limit of $\beta \to 0$ or $\beta \to \infty$ the normalized escape rate κ tends to zero, while for some intermediate value of β there exists a maximum. After having clarified these qualitative similarities between the Markovian and the non-Markovian case, attention should now be directed to the quantitative differences.

For increasing correlation times the respective curves are shifted to the right and the values of the maxima gradually decrease. However, this decrease of the maximal value only appears for higher correlation times. The shift to the right, on the one hand, consequently leads to systematically higher escape rates for strong friction in case of increasing correlation times (see Fig. 11). On the other hand, this leads to an effective decrease of the escape rate for weak friction. Both the increase and decrease of the escape rate for strong and weak coupling β, are consequences of an effective reduction of the friction rate β for increasing correlation times. This effect is mentioned in Ref. [54], where the influence of a non-Markovian correlation function on the diffusion over an inverse parabolic potential is investigated. In this context an ensemble of Brownian particles is initialized at $x_0 < 0$ to the left of a potential barrier, symmetrically located around $x = 0$. On that basis an expression for the overpassing probability over the barrier for fixed initial conditions,

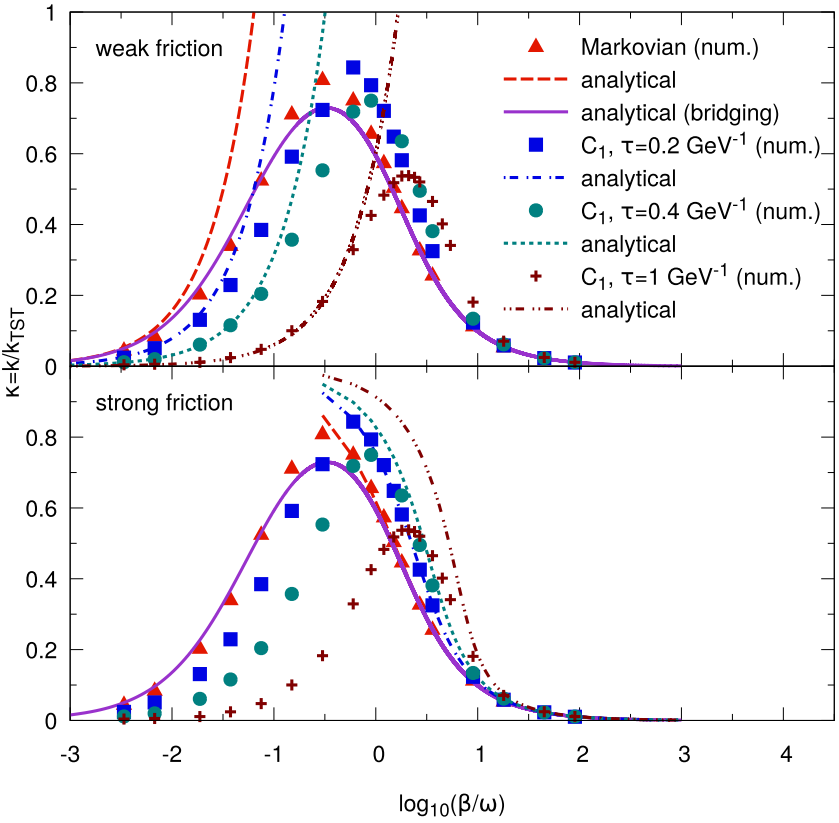

Fig. 11. Comparison of the normalized steady-state escape rate κ as a function of the dimensionless parameter $\frac{\beta}{\omega_b}$ for correlation functions C_0 and C_1 (Eqs. (132) and (12)), where $E_b = 2.5\,\text{GeV}$, $\omega_b = 5\,\text{GeV}$, $m = 1.11\,\text{GeV}$, and $T = 1\,\text{GeV}$. Analytical results are computed, using Eqs. (30) and (46) in the weak-friction, Eqs. (33) and (47), with λ_{NM} given in Appendix B, in the strong-friction regime and Eq. (36) for the bridging between strong- and weak-friction regime.

x_0 and v_0, in the limit of $\lambda_{\text{M}} t \gg 1$ or $\lambda_{\text{NM}} t \gg 1$ is derived for correlation functions C_0 and C_1 (Eqs. (132) and (12)), respectively [31,54]:

$$F(t; x_0, v_0) = \frac{1}{2}\text{erfc}\left(\frac{\omega}{\sqrt{\beta\lambda_{\text{M}}}}\left[\sqrt{\frac{B}{T}} - \frac{\lambda_{\text{M}}}{\omega}\sqrt{\frac{K}{T}}\right]\right), \tag{141}$$

$$F(t; x_0, v_0) = \frac{1}{2}\text{erfc}\left(\frac{\omega\sqrt{1+\lambda_{\text{NM}}\tau}}{\sqrt{\beta\lambda_{\text{NM}}}}\left[\sqrt{\frac{B}{T}} - \frac{\lambda_{\text{NM}}}{\omega}\sqrt{\frac{K}{T}}\right]\right). \tag{142}$$

Hereby, K denotes the initial kinetic energy of a Brownian particle, i.e. $K = \frac{1}{2}mv_0^2$, B is the height of the barrier the Brownian particle needs to overcome, starting from position x_0, i.e. $B = \frac{1}{2}m\omega^2 x_0^2$, ω is the barrier frequency, and λ_{M} and λ_{NM} designate the quantities, indicated in the context of the Markovian and non-Markovian model of Kramers' escape rate problem (see Eqs. (34) and (48)), where λ_{NM} is derived in Appendix B. Given these stationary overpassing probabilities, it is straightforward to compute an initial kinetic energy the Brownian particle must possess to overcome the potential barrier with a probability of 50%, setting the expressions in parentheses

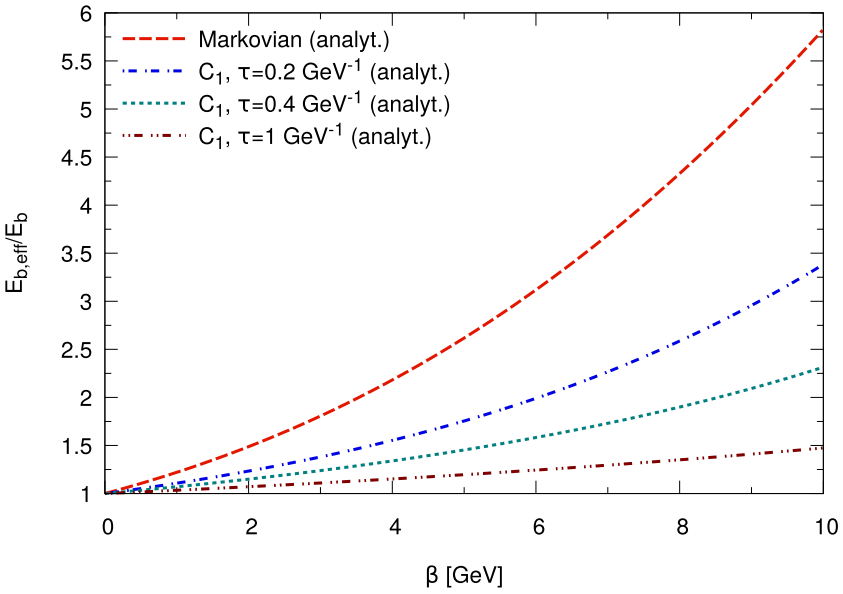

Fig. 12. Effective barrier height $E_{b,\mathrm{eff}}$ (Eqs. (145) and (146)) normalized to the barrier height E_b as a function of the coupling β for different correlation times τ.

to zero. For correlation function C_0 this is

$$K := B_\mathrm{eff} = \left(\frac{\omega}{\lambda_\mathrm{M}}\right)^2 B, \tag{143}$$

and for correlation function C_1 the appropriate initial kinetic energy K is given by

$$K := B_\mathrm{eff} = \left(\frac{\omega}{\lambda_\mathrm{NM}}\right)^2 B. \tag{144}$$

To relate the results of Ref. [54] to the simulations of this work, B needs to be replaced by the barrier height E_b of the composite potential, Eq. (130), the Brownian particle has to overcome, starting at the bottom of the initial well (see Fig. 6), i.e.

$$B_\mathrm{eff} \approx E_{\mathrm{b,eff}} = \left(\frac{\omega}{\lambda_\mathrm{M}}\right)^2 E_\mathrm{b}, \tag{145}$$

$$B_\mathrm{eff} \approx E_{\mathrm{b,eff}} = \left(\frac{\omega}{\lambda_\mathrm{NM}}\right)^2 E_\mathrm{b}. \tag{146}$$

Certainly, this is just an approximation but it does not change the qualitative implications:

Comparing the ratio $\frac{E_{b,\mathrm{eff}}}{E_\mathrm{b}}$ in the Markovian and non-Markovian limit as a function of the coupling β it can be concluded that the effective barrier height $E_{b,\mathrm{eff}}$ systematically reduces for increasing correlation times and fixed β (see Fig. 12). This reduction of the effective barrier height for fixed β and increasing correlation times in turn is equivalent to an effective reduction of the friction. Hence, it can be assumed that the average behavior of a considered ensemble in case of a non-Markovian noise is basically the same as in case of a Markovian noise, but with a friction rate β being effectively reduced (see Fig. 12).

At least for the low-friction regime this effective reduction of the friction rate β can be directly seen from the approximate analytical formula computed with Eq. (46), which will be explained in

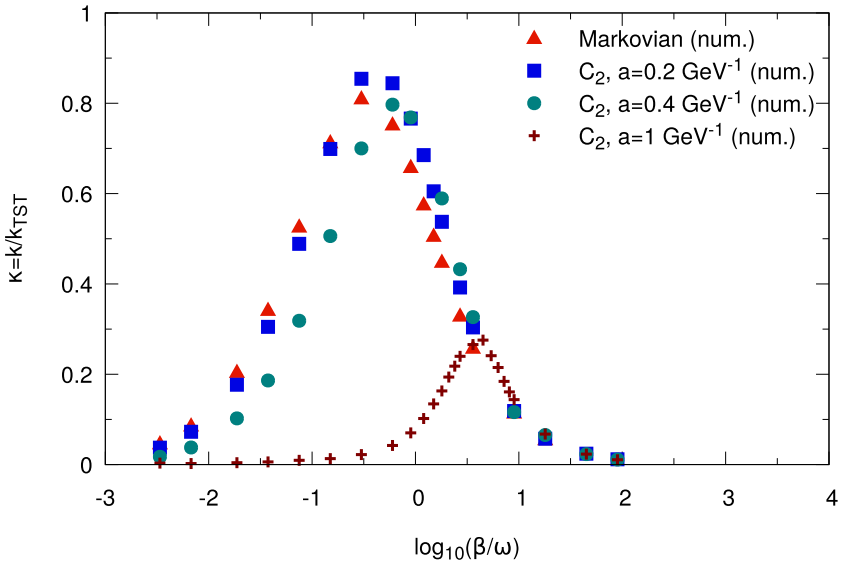

Fig. 13. Comparison of the normalized steady-state escape rate κ as a function of the dimensionless parameter $\frac{\beta}{\omega_b}$ for correlation functions C_0 and C_2 (Eqs. (132) and (13)), where $E_b = 2.5\,\text{GeV}$, $\omega_b = 5\,\text{GeV}$, $m = 1.11\,\text{GeV}$, and $T = 1\,\text{GeV}$.

detail in Section 4.5. Taking now the formulas for the weak- and the strong-friction regime in case of Kramers' classical escape rate problem (see Eqs. (30) and (35)) it is straightforward to understand how increasing correlation times lead to smaller escape rates for weak friction and higher escape rates for strong friction. Furthermore increasing correlation times are responsible for the shift of the curves, since for higher correlation times higher values for β are required for the strong-friction regime to be valid.

4.4.2. Correlation function C_2

Again, the depicted curves for correlation function C_2 (Eq. (13)) exhibit the expected bell-shaped form (see Fig. 13). As for correlation function C_1, the above-mentioned effects of increasing correlation times compared to the Markovian case are observed, i.e. the shift to the right, the decrease of the maximum, smaller escape rates for weak friction and higher escape rates for strong friction. In contrast to correlation function C_1 the shift is comparatively tiny for smaller correlation times ($a = 0.2\,\text{GeV}^{-1}$ and $a = 0.4\,\text{GeV}^{-1}$), leading to less deviation from the Markovian case (see Fig. 13). For a large correlation time ($a = 1\,\text{GeV}^{-1}$), however, the shift is even greater than for a large correlation time ($\tau = 1\,\text{GeV}^{-1}$) in case of correlation function C_1 (see Figs. 11 and 13). Even though, because of a lack of analytical results for correlation function C_2, no exact information exists about the behavior of β with regard to increasing correlation times, it is reasonable to assume a similar behavior as for correlation function C_1. However, this effective reduction of the friction for increasing correlation times seems to be much more significant for higher correlation times (see Fig. 13).

4.4.3. Correlation function C_3

The numerical studies for correlation function C_3, Eq. (14), need to be considered separately from the previous ones. Unlike before, the steady-state escape rate is not examined as a function of the coupling β but of the dimensionless coupling g (see Fig. 14). For this particular correlation function (see Eq. (14)) no strict Markovian limit exists as the Fourier transform vanishes in the limit of $\omega \to 0$ (see Eq. (17)). For that reason, only correlation function C_3 is investigated here for different correlation times. A number of the peculiarities of correlation function C_3 is discussed in Appendix C.

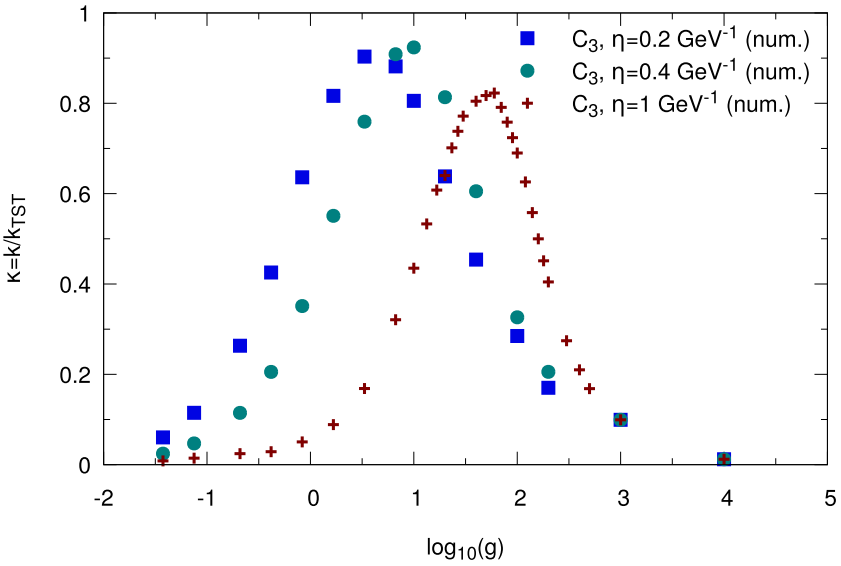

Fig. 14. Normalized steady-state escape rate κ as a function of the dimensionless coupling g for correlation function C_3 (Eq. (14)) and different values of correlation time η (Eq. (C.3)), where $E_b = 2.5\,\text{GeV}$, $\omega_b = 5\,\text{GeV}$, $m = 1.11\,\text{GeV}$, and $T = 1\,\text{GeV}$.

Although in many respects very different from correlation function C_1 and C_2 (see Appendix C), even for correlation function C_3 the different curves obey the above-mentioned bell-shaped behavior. Furthermore, as for correlation functions C_1 and C_2, a shift of the curves for increasing correlation times can be observed, connected to the same implications as for the other correlation functions. Different from before the value of the maximum seems to reduce very slowly, as even for high correlation times the maximum only lies slightly below the maxima for smaller correlation times (see Fig. 14). It is remarkable that for small correlation times the steady-state escape rate comes very close to the TST-rate, much closer than in case of correlation functions C_1 and C_2. Taking all results together, it is again reasonable to assume that increasing correlation times lead to an effective reduction of the actual friction β.

4.5. Comparison of analytical with numerical results

After having clarified that the numerical algorithm used in this work is accurate (see Section 4.3), the aim of this subsection is to discuss the accuracy of the approximate analytical solutions (see Eqs. (30), (33), (35), (36), (46), and (47) with λ_{NM} given in Appendix B), compared to the numerical results, presented above. In doing so, the limits of validity of the approximate analytic formulas are demonstrated. It should be recalled here that in the weak-friction regime the Brownian particle is subject to an almost frictionless, deterministic oscillatory movement inside the initial potential well (see Figs. 3 and 6) which corresponds to a harmonic oscillator. Therefore, the action I at energy E_b, a term common to the approximate analytic formulas in the weak-friction regime, Eqs. (30) and (46), is given by:

$$I(E_b) = \frac{2\pi E_b}{\omega}. \tag{147}$$

Starting first with the comparison in the intermediate-to-strong-friction regime (see Fig. 11), for a small correlation time, $\tau = 0.2\,\text{GeV}^{-1}$, the Markovian and the non-Markovian simulations (correlation functions C_0 and C_1; Eqs. (132) and (12)) show very good consistency with the analytical results (Eqs. (33), (35), and (47) with λ_{NM} given in Appendix B). Deviations from the analytical

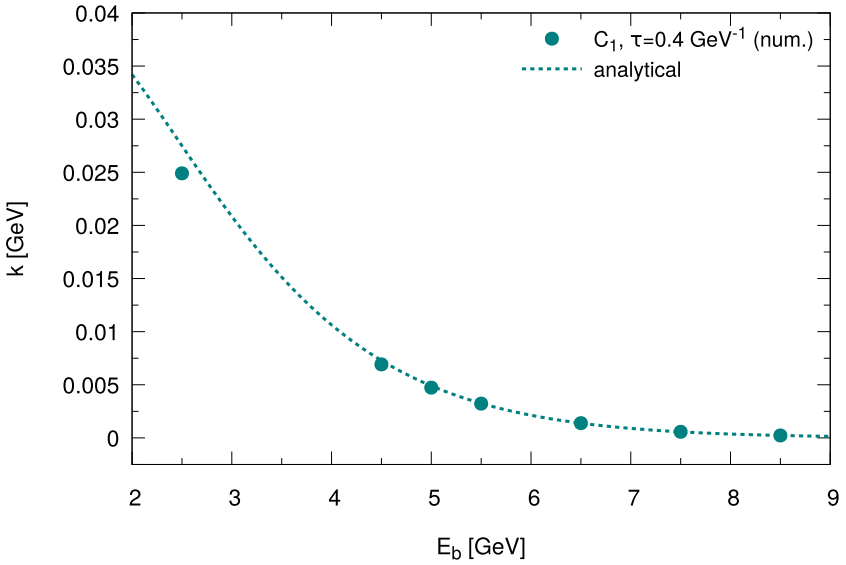

Fig. 15. Steady-state escape rate k as a function of the barrier height E_b, where $\beta = 18\,\mathrm{GeV}$, $m = 1.11\,\mathrm{GeV}$, and $T = 1\,\mathrm{GeV}$. The analytical solution is generated using Eq. (47) with λ_NM given in Appendix B.

results are not greater than 2% and within the error bars. The obtained accuracy could be further improved by use of smaller time steps Δt. For increasing correlation times, $\tau = 0.4\,\mathrm{GeV}^{-1}$ and $\tau = 1\,\mathrm{GeV}^{-1}$, however, the accuracy is steadily decreasing. While the deviation of the numerical and analytical results is about 10% for $\tau = 0.4\,\mathrm{GeV}^{-1}$, the discrepancy is even greater (about 30%) for $\tau = 1\,\mathrm{GeV}^{-1}$. This growing divergence for increasing correlation times is most likely due to fact that Eq. (47) is not longer applicable. In fact, it can be shown that Eq. (47) becomes valid again for larger barrier heights E_b. As an example, Fig. 15 demonstrates how the accuracy of the numerical results for a fixed choice of parameters is improved by increasing the barrier height E_b. Beginning with a deviation of about 10% for $E_\mathrm{b} = 2.5$ GeV the discrepancy reduces gradually to less than 1% for $E_\mathrm{b} = 8.5$ GeV.

In the weak-friction regime the accuracy of the Markovian simulations compared to the analytical results, evaluated with Eq. (30), is worse than in the strong-friction regime. Here only the first two points on the left side approximately match with the analytical result. The deviation of the first point located to the outermost left is about 10%, the second point already deviates about 20%. This higher deviation can be attributed to the fact that on the one hand the time step Δt is too large and on the other hand that the condition $E_\mathrm{b} \gg k_\mathrm{B}T$ for Eq. (30) to be valid is not fulfilled properly. Especially condition $E_\mathrm{b} \gg k_\mathrm{B}T$ seems to have a stronger effect on the validity of Eq. (30) which can be clarified by means of the classical-rate phase diagram (see Fig. 4). Apparently the range of validity of Eq. (30) becomes smaller, the smaller the ratio $\frac{k_\mathrm{B}T}{E_\mathrm{b}}$. This explains the observation that the analytical results only fit the numerical results for very small friction values.

In contrast to that, in the non-Markovian case the accordance between numerical and analytical results (see Eq. (46)) improves for increasing correlation times (see Fig. 11). Growing correlation times seem to enlarge the range of validity of Eq. (46) step by step, leading to a very good consistency until close to the maximum of the rate. It should be noticed here that the approximate analytical results (see Eq. (46)) were evaluated under the assumption that the initial well is an ideal harmonic oscillator. This is a reasonable approximation for the potential field used for the simulations (see Eq. (130)). In this case, computing $\epsilon(I_\mathrm{B})$ (see Eq. (43)) and inserting it into Eq. (46) results in

$$k_{A\to C} = \frac{\beta}{1+\tau^2\omega^2}\frac{I(E_\mathrm{b})}{k_\mathrm{B}T}\frac{\omega_a}{2\pi}\exp\left[-\frac{E_\mathrm{b}}{k_\mathrm{B}T}\right], \tag{148}$$

where $I(E_b)$ is again given by Eq. (147). This corresponds to the classical steady-state escape rate in the weak-friction regime (Eq. (30)) but with the damping rate β being reduced by a factor of $\frac{1}{1+\tau^2\omega^2}$, which can be essentially identified with the Fourier transform of correlation function C_1 (see Eq. (15)). Basically, the effective damping in the weak-friction regime is obtained by substituting the damping γ by $\tilde{\Gamma}(\omega = \omega_a)/2$ in the linear harmonic approximation as an effectively well-defined Markovian description [11,13,14].

This in fact supports the statement, at least for correlation function C_1 in the low-friction regime, that the main difference between the Markovian and non-Markovian escape rate is the effective reduction of the friction rate for increasing correlation times.

Summing up the results for the low- and the strong-friction regime, there obviously exist two opposite effects on the validity of formulas (46) and (47) concerning increasing correlation times. On the one hand rising correlation times lead to improving accordance between numerical and analytical results in the weak-friction limit. On the other hand accordance becomes worse in the intermediate-to-strong-friction regime. To obtain a comparably good consistency in both limiting regimes either the barrier height E_b has to be increased (see also Fig. 15) or the temperature T has to be decreased.

Finally, only the comparison of the bridging formula, Eq. (36) with the numerical results of the Markovian simulations (i.e. using correlation function C_0, see Eq. (132)) remains. First of all, it should be mentioned that the simple ad hoc formula, Eq. (36), in fact yields the expected bell-shaped curve. Furthermore good accordance in both limiting regimes can be seen as expected from the construction of formula (36) (see Fig. 11). Even the points to the left of the maximum, which were not fitted properly by the steady-state escape rate in the weak-friction limit, Eq. (30), are approximately covered (see Fig. 11). The difference between analytical and numerical results here is about 12%, which is the usual deviation between numerical and analytical results, obtained by other researchers using different numerical approaches [28]. Moreover, the second point to the outermost left is fitted more accurately by the bridging formula, Eq. (36), compared to the analytical equation for the weak-friction escape rate, Eq. (30). While the discrepancy between numerical and analytical results is about 20% for Eq. (30), the difference reduces to about 10% for Eq. (36). This in fact seems to substantiate the above-mentioned assumption that Eq. (30) is not longer valid for the appropriate damping rate.

5. Conclusions

In this work Kramers' steady-state escape rate has been computed numerically as a function of the damping rate β in the case of a Markovian noise C_0, Eq. (132), and three non-Markovian noise variants, C_1, C_2 and C_3, cf. Eqs. (12)–(14), solving the appropriate Markovian or non-Markovian GLE, Eq. (40), with the three-step Adams–Bashforth method, indicated in Section 4. Hereby the numerical implementation [31] of the algorithm, depicted in Section 2, is used to generate the non-Markovian noise, given a symmetric and exponentially decaying correlation function.

A first objective then has been to validate the numerical algorithm by adjusting the numerical parameters such that the approximate analytic formulas for correlation functions C_0 and C_1, cf. Eqs. (132) and (12) are accurate and comparing analytical with numerical results (see Section 4.3). Furthermore the limits of validity of the approximative analytic formulas are discussed in Section 4.5. Overall it appears that there is good consistency between numerical and analytical results. Appearing deviations – in the weak-friction regime not larger than 10% and in the strong-friction regime less than 2% – are the consequence of the invalidity of the approximative analytic formulas, Eqs. (30), (33), (35), (46), and (47), where λ_{NM} is given in Appendix B, and not of the incorrectness of numerical results. By suitable selection of the relevant parameters (barrier height E_b, temperature T, size of time steps Δt) the accordance can be further increased at the expense of higher computation times.

After having established that the numerical algorithm indeed works well, the main objective of this work has been to identify the differences of Kramers' steady-state escape rate for white and colored noise for the different correlation functions and to provide a possible explanation for these differences.

It turns out that growing correlation times lead to a decrease of the steady-state escape rate in the weak-friction regime and to an increase in the intermediate-to-strong-friction regime for fixed values of the damping rate β for correlation functions C_1 and C_2, cf. Eqs. (12) and (13). In the case of correlation function C_1, for which analytical results exist, both effects are identified to be the consequences of an effective reduction of the friction for increasing correlation times. Since correlation function C_2 qualitatively obeys the same behavior, it is reasonable to assume the same explanation. However, this should be verified by an analytical treatment of correlation function C_2. Again, it should be emphasized that the temperature T is an external parameter which remains constant during the evolution of the system since the thermal bath, the Brownian particle is exposed to, is assumed to be in thermodynamic equilibrium. However, the numerical algorithm would also apply to a background medium in local thermodynamic equilibrium for a spacetime-dependent temperature.

Furthermore, special attention should be payed to correlation function C_3, Eq. (14). Although rather similar behavior of the steady-state escape rate as a function of the dimensionless coupling g (not β for correlation function C_3) for growing correlation times is obtained, correlation function C_3 obeys some special features, compared to correlations functions C_1 and C_2, which are discussed in Appendix C. Next to a vanishing Fourier transform $\tilde{\Gamma}(\omega) = 0$ for $\omega = 0$, solving the GLE for a free Brownian particle, Eq. (40), where the potential term is neglected, with correlation function C_3 yields different peculiarities: There is a non-vanishing retarded Green's function $G_{\mathrm{ret}}(t)$ for $t \to \infty$, the equipartition theorem becomes invalid and the equilibrium velocity distribution function seems to obey a Boltzmann distribution but with a temperature being reduced by a certain factor (see Appendix C). However, as is shown in Appendix C, the equipartition theorem becomes again valid for a bound Brownian particle.

Altogether it can be stated that the numerical algorithm essentially based on the three-step Adams–Bashforth method and the generation of a colored, non-Markovian thermal noise is perfectly applicable to Kramers' classical escape rate problem and can be, differently from the approximate analytical formulas (30), (33), (35), (46), and (47), employed for arbitrarily shaped potentials and correlation functions over the whole friction range – weak, strong and most importantly friction values in between – without the need of any additional corrections, resulting for example from anharmonicities of the potential [40–42] (see also Section 3.2).

Acknowledgments

We thank S. Leupold for fruitful discussions about the dissipation kernel C_3 and J. Schmidt for providing his C^{++} implementation of colored noise. B.S. acknowledges support through the Helmholtz Graduate School for Hadron and Ion Research for FAIR (HGS-HIRe), Germany and financial support within the framework of the cooperation between GSI Helmholtz Centre for Heavy Ion Research and Goethe-Universität Frankfurt am Main (GSI F&E program), Germany. We are grateful to the LOEWE Center for Scientific Computing (LOEWE-CSC) at Frankfurt for providing computing resources. We also acknowledge support by the Deutsche Forschungsgemeinschaft (DFG, German Research Foundation) through the grant CRC-TR 211 'Strong-interaction matter under extreme conditions' - Project number 315477589 - TRR 211. Z.X.'s work was financially supported by the National Natural Science Foundation of China under Grants No. 11575092 and No. 11890712.

Appendix A. One-dimensional Laplace transform (LT)

Dealing with initial value problems the application of Laplace transforms is a very effective tool. This section is devoted to the fundamental principles of the Laplace transform. Furthermore, several useful Laplace transforms are indicated.

Definition. Given a mapping in the form of

$$f : [0, \infty) \to \mathbb{C}, \quad t \mapsto f(t), \tag{A.1}$$

being at least piecewise continuous and of exponential order, where the latter means that regarding to two constants $M,\ \alpha \in \mathbb{R}$ the condition

$$|f(t)| \leq Me^{\alpha t} \tag{A.2}$$

holds [55]. Then the Laplace transform and its corresponding inverse are given by [55,56]:

$$\mathcal{L}[f](s) = \int_0^\infty f(t) \cdot e^{-st}\,\mathrm{d}t := F(s), \quad s \in \mathbb{C}, \tag{A.3}$$

$$\mathcal{L}^{-1}[F](t) = \lim_{\omega\to\infty} \frac{1}{2\pi i} \int_{s-i\omega}^{s+i\omega} F(s) \cdot e^{st}\,\mathrm{d}s = \begin{cases} 0 & t < 0 \\ f(t) & t \geq 0. \end{cases} \tag{A.4}$$

The LT of function f exists for $\mathrm{Re}(s) > \mathrm{Re}(\alpha)$ due to condition (A.2)

Properties. In accordance with their definitions in Eqs. (A.3) and (A.4) the LT and its corresponding inverse are linear transformations. Let there be two functions $g(t)$ and $f(t)$, for which both the Laplace transforms and their corresponding back-transforms exist. Then for two arbitrary constants $a,\ b \in \mathbb{C}$ the following relations hold:

$$\mathcal{L}[a \cdot f(t) + b \cdot g(t)] = a \cdot \mathcal{L}[f](s) + b \cdot \mathcal{L}[g](s), \tag{A.5}$$

$$\mathcal{L}^{-1}[a \cdot F(s) + b \cdot G(s)] = a \cdot \mathcal{L}^{-1}[F](t) + b \cdot \mathcal{L}^{-1}[G](t). \tag{A.6}$$

Useful transformations. Let there exist two Laplace transformable functions $g(t)$ and $f(t)$, then the following applies:

1. **Exponential function, $a \in \mathbb{C}$ (arbitrary)**

$$\mathcal{L}[e^{at}](s) = \int_0^\infty e^{-(s-a)t}\,\mathrm{d}t = \frac{1}{s-a}, \quad \mathrm{Re}(s) > \mathrm{Re}(a) \tag{A.7}$$

2. **Convolution**

$$\mathcal{L}\left[\int_0^t f(t-\tau)g(\tau)\,\mathrm{d}\tau\right](s) = \int_0^\infty \left(\int_0^t f(t-\tau)g(\tau)\,\mathrm{d}\tau\right) e^{-st}\,\mathrm{d}t = F(s)G(s) \tag{A.8}$$

3. **Time derivative**

$$\mathcal{L}\left[\frac{\mathrm{d}}{\mathrm{d}t}f(t)\right](s) = \int_0^\infty \left(\frac{\mathrm{d}}{\mathrm{d}t}f(t)\right) e^{-st}\,\mathrm{d}t = sF(s) - f_0 \tag{A.9}$$

Appendix B. λ_{NM} For correlation function C_1

In this section the prefactor λ_{NM} of the escape rate in the spatial-diffusion regime (see Eq. (47)) will be derived for correlation function C_1, Eq. (12). For this purpose the roots of the function

$$f(\lambda) = \lambda^2 - \omega_b^2 + \frac{\tilde{\Gamma}(\lambda)}{m}\lambda \tag{B.1}$$

have to be computed. Thereby, Γ is related to the correlation function C_1 by the second fluctuation–dissipation theorem (see Eq. (41)). Taking correlation function C_1 (see Eq. (12)), Γ is readily obtained as

$$\Gamma(|t|) = \frac{D}{2k_{\mathrm{B}}T\tau} \exp\left[-\frac{|t|}{\tau}\right] = \frac{\gamma}{\tau} \exp\left[-\frac{|t|}{\tau}\right], \tag{B.2}$$

where from the first to the second step the fluctuation–dissipation relation has been employed. Performing the LT of Γ, using Eq. (A.7), one obtains

$$\tilde{\Gamma}(\lambda) = \mathcal{L}\left[\frac{\gamma}{\tau} \exp\left[-\frac{|t|}{\tau}\right]\right] = \frac{\gamma}{\tau\lambda + 1}. \tag{B.3}$$

Subsequent insertion of Eq. (B.3) in function (B.1) leads to

$$f(\lambda) = \lambda^2 - \omega_b^2 + \frac{\beta\lambda}{\tau\lambda + 1}. \tag{B.4}$$

To obtain λ_{NM} the next task will be to identify the roots of (B.4)

$$\lambda^2 - \omega_b^2 + \frac{\beta\lambda}{\tau\lambda + 1} = 0, \tag{B.5}$$

using Cardano's formula. To this end, the algorithm indicated in Ref. [57] is applied on the above equation. First, however, Eq. (B.5) must be transformed into the form,

$$\lambda^3 + a\lambda^2 + b\lambda + c = 0, \tag{B.6}$$

where

$$a = \frac{1}{\tau}, \tag{B.7}$$

$$b = \frac{\beta}{\tau} - \omega_b^2, \tag{B.8}$$

$$c = -\frac{\omega_b^2}{\tau}. \tag{B.9}$$

Dependent on the expression

$$D = \left(\frac{q}{2}\right)^2 + \left(\frac{p}{3}\right)^3, \tag{B.10}$$

where

$$p = b - \frac{a^2}{3} \tag{B.11}$$

and

$$q = \frac{2a^3}{27} - \frac{ab}{3} + c, \tag{B.12}$$

there are three different cases for the solution of Eq. (B.5), supposing $p \neq 0$ [57]:

1. $D > 0$: One real root and two complex conjugate roots,
2. $D = 0$: Three real roots (one double root),
3. $D < 0$: Three distinct real roots.

Subsequently, the solutions for the three different cases for D, using the above relations for a, b, c, p, and q (see Eqs. (B.7), (B.8), (B.9), (B.11), and (B.12)), are indicated:

$D > 0$:

$$\begin{aligned} \lambda_1 &= A + B - \frac{a}{3}, \\ \lambda_{2,3} &= -\frac{A+B}{2} \pm \frac{A-B}{2}\mathrm{i}\sqrt{3} - \frac{a}{3}, \end{aligned} \tag{B.13}$$

where

$$\begin{aligned} A &= \sqrt[3]{-\frac{q}{2} + \sqrt{D}}, \\ B &= \sqrt[3]{-\frac{q}{2} - \sqrt{D}}. \end{aligned} \tag{B.14}$$

$D = 0$:

$$\begin{aligned} \lambda_1 &= \sqrt[3]{-4q} - \frac{a}{3}, \\ \lambda_{2,3} &= \sqrt[3]{\frac{q}{2}} - \frac{a}{3}. \end{aligned} \tag{B.15}$$

$D < 0$:

$$\begin{aligned}\lambda_1 &= 2\sqrt{-\frac{p}{3}}\cos\left(\frac{\theta}{3}\right) - \frac{a}{3},\\ \lambda_2 &= -2\sqrt{-\frac{p}{3}}\cos\left(\frac{\theta}{3} - \frac{\pi}{3}\right) - \frac{a}{3},\\ \lambda_3 &= -2\sqrt{-\frac{p}{3}}\cos\left(\frac{\theta}{3} + \frac{\pi}{3}\right) - \frac{a}{3},\end{aligned} \tag{B.16}$$

where

$$\theta = \arccos\left(-\frac{q}{2}\sqrt{-\frac{27}{p^3}}\right). \tag{B.17}$$

For a more detailed discussion of the roots of the particular function, Eq. (B.4), reference is made to Ref. [54]. The quantity λ_{NM} is then given by the largest positive root λ_1 of Eqs. (B.13), (B.15), or (B.16), respectively. From the above expressions it can be furthermore concluded that λ_{NM} is a function of β, ω_b, and τ, i.e. $\lambda_{\mathrm{NM}} = \lambda_{\mathrm{NM}}(\beta, \omega_b, \tau)$.

Appendix C. Peculiarities of correlation function C_3

An interesting dissipation kernel, bearing very special features and being related to correlation function C_3, cf. Eq. (14), via the second fluctuation–dissipation theorem, Eq. (41), is written as

$$\Gamma(|t|) = \frac{g}{4}\alpha^2\left(1 - \frac{\alpha}{\sqrt{m}}|t|\right)\exp\left(-\frac{\alpha}{\sqrt{m}}|t|\right). \tag{C.1}$$

Its Fourier transform is given by

$$\tilde{\Gamma}(\omega) = \frac{g\alpha^3\omega^2}{\sqrt{m}\left(\omega^2 + \frac{\alpha^2}{m}\right)^2} = \frac{g\alpha^3\omega^2}{\sqrt{m}\left(\omega + \frac{i\alpha}{\sqrt{m}}\right)^2\left(\omega - \frac{i\alpha}{\sqrt{m}}\right)^2}, \tag{C.2}$$

which was computed using Eq. (19). From Eq. (C.1) the correlation time for correlation function C_3 is immediately obtained,

$$\eta := \frac{\sqrt{m}}{\alpha}. \tag{C.3}$$

The dissipation kernel $\Gamma(t)$ and its Fourier transform $\tilde{\Gamma}(\omega)$ are depicted in Fig. C.16. Relating to this Fourier transform (C.2) the first particular property of the underlying correlation function emerges: For $\omega = 0$ the Fourier transform of Eq. (C.1) equals zero in contrast to the other two correlation functions C_1 and C_2 (see Eqs. (12) and (13)). Additionally, the dissipation kernel $\Gamma(t)$ of correlation function C_3 drops significantly below zero until it reaches a minimum and increases again, approaching zero for $t \to \infty$. Such a dissipative kernel for the damping is rather typical in a quantum field theoretical setting with a self-interacting theory like a scalar Φ^4-theory (see e.g. Ref. [14]). Further particularities arise by solving the GLE with dissipation kernel (C.1) for a free Brownian particle, i.e.

$$\dot{v} + \frac{1}{m}\int_0^t \Gamma(t - t')v(t')\mathrm{d}t' = \frac{\xi(t)}{m}, \tag{C.4}$$

using the method of Green's functions. However, before applying the method of Green's functions to the latter equation several modifications of it have to be made, leading to

$$\dot{v} + \frac{1}{m}\int_{-\infty}^{\infty} \underbrace{\Gamma(t - t')\Theta(t - t')}_{:=\mathrm{i}\Pi_{\mathrm{ret}}(t-t')} v(t')\mathrm{d}t' = \frac{\xi(t)}{m}. \tag{C.5}$$

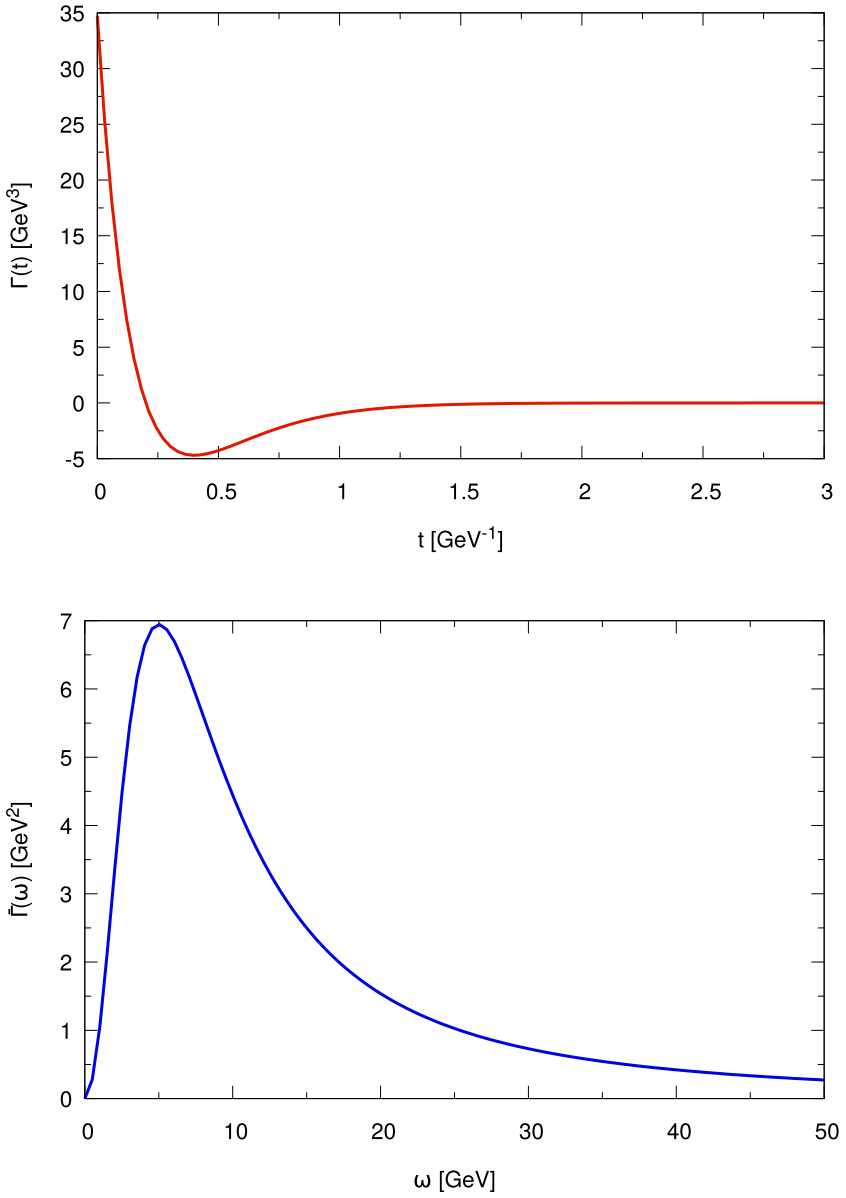

Fig. C.16. Dissipation kernel $\Gamma(t)$ (upper figure; Eq. (C.1)) and its Fourier transform $\tilde{\Gamma}(\omega)$ (lower figure; Eq. (C.2)), where $g = 5$, $m = 1.11\,\mathrm{GeV}$, and $\eta = 0.2\,\mathrm{GeV}^{-1}$.

From Eq. (C.4) to (C.5) the upper integration border has been extended to ∞ by including the Heaviside function into the integral. The lower integration border can be extended to $-\infty$, assuming that $v(t) = 0$ for $t < 0$.

Using now the method of Green's functions the starting point is

$$\dot{G}_{\mathrm{ret}}(t) + \frac{i}{m}\int_{-\infty}^{\infty} \Pi_{\mathrm{ret}}(t-t')G_{\mathrm{ret}}(t')\mathrm{d}t' = \delta(t). \tag{C.6}$$

The Fourier transform of this equation reads

$$-i\omega\tilde{G}_{\mathrm{ret}} + \frac{i}{m}\tilde{\Pi}_{\mathrm{ret}}(\omega)\tilde{G}_{\mathrm{ret}}(\omega) = 1. \tag{C.7}$$

Proceeding further, by solving Eq. (C.7) for $\tilde{G}_{\mathrm{ret}}$, the solution to the actual problem (see Eq. (C.6)) is obtained by performing the inverse Fourier transform of

$$\tilde{G}_{\mathrm{ret}} = \frac{\mathrm{i}}{\omega - \frac{1}{m}\tilde{\Pi}_{\mathrm{ret}}}. \tag{C.8}$$

But before applying the inverse Fourier transform, first one has to determine $\tilde{\Pi}_{\mathrm{ret}}$, defined in Eq. (C.5), as

$$\mathrm{i}\Pi_{\mathrm{ret}}(t) = \Gamma(t)\Theta(t). \tag{C.9}$$

By use of the convolution theorem, $\mathrm{i}\tilde{\Pi}_{\mathrm{ret}}$ is given by

$$\mathrm{i}\tilde{\Pi}_{\mathrm{ret}} = \frac{1}{2\pi}\int_{-\infty}^{\infty}\tilde{\Gamma}(\omega')\tilde{\Theta}(\omega-\omega')\mathrm{d}\omega'. \tag{C.10}$$

Insertion of Eq. (C.2) into Eq. (C.10) then leads to

$$\mathrm{i}\tilde{\Pi}_{\mathrm{ret}} = \frac{\mathrm{i}g\alpha^3}{2\pi\sqrt{m}}\int_{-\infty}^{\infty}\underbrace{\frac{\omega'^2}{\left(\omega'+\frac{\mathrm{i}\alpha}{\sqrt{m}}\right)^2\left(\omega'-\frac{\mathrm{i}\alpha}{\sqrt{m}}\right)^2}\frac{1}{\omega-\omega'+\mathrm{i}\epsilon}}_{:=f(\omega')}\mathrm{d}\omega'. \tag{C.11}$$

The integral on the right-hand side of Eq. (C.11) can be computed by means of the theorem of residues,

$$\mathrm{i}\tilde{\Pi}_{\mathrm{ret}} = \frac{g\alpha^3}{\sqrt{m}}\lim_{\omega'\to-\frac{\mathrm{i}\alpha}{\sqrt{m}}}\frac{\mathrm{d}}{\mathrm{d}\omega'}\left(\left(\omega'+\frac{\mathrm{i}\alpha}{\sqrt{m}}\right)^2 f(\omega')\right). \tag{C.12}$$

Evaluating Eq. (C.12) a compact form for $\tilde{\Pi}_{\mathrm{ret}}$ is obtained:

$$\tilde{\Pi}_{\mathrm{ret}} = \frac{g\alpha^2\omega}{4\left(\omega+\frac{\mathrm{i}\alpha}{\sqrt{m}}\right)^2}. \tag{C.13}$$

With Eq. (C.13) the Fourier transform of the retarded Green's function (C.8) is given by

$$\tilde{G}_{\mathrm{ret}} = \frac{\mathrm{i}\left(\omega+\frac{\mathrm{i}\alpha}{\sqrt{m}}\right)^2}{\omega\left(\omega-\frac{\sqrt{g}\alpha}{2\sqrt{m}}+\frac{\mathrm{i}\alpha}{\sqrt{m}}\right)\left(\omega+\frac{\sqrt{g}\alpha}{2\sqrt{m}}+\frac{\mathrm{i}\alpha}{\sqrt{m}}\right)}. \tag{C.14}$$

Now that all ingredients are together, the retarded Green's function G_{ret} can be computed by inverse Fourier transform of Eq. (C.14):

$$\begin{aligned} G_{\mathrm{ret}}(t) &= \frac{1}{2\pi}\int_{-\infty}^{\infty}\tilde{G}_{\mathrm{ret}}(\omega)\exp\left(-\mathrm{i}\omega t\right)\mathrm{d}\omega \\ &= \frac{1}{2\pi}\int_{-\infty}^{\infty}\frac{\mathrm{i}\left(\omega+\frac{\mathrm{i}\alpha}{\sqrt{m}}\right)^2}{\omega\left(\omega-\frac{\sqrt{g}\alpha}{2\sqrt{m}}+\frac{\mathrm{i}\alpha}{\sqrt{m}}\right)\left(\omega+\frac{\sqrt{g}\alpha}{2\sqrt{m}}+\frac{\mathrm{i}\alpha}{\sqrt{m}}\right)}\exp\left(-\mathrm{i}\omega t\right)\mathrm{d}\omega \\ &= \frac{1}{2\pi}(-2\pi\,\mathrm{i})\sum_{i=1}^{3}\mathrm{res}_{\omega_i}g(\omega), \end{aligned} \tag{C.15}$$

where the third equal sign follows making again use of the residue theorem.

This finally leads to

$$G_{\mathrm{ret}}(t) = \frac{1}{4+g}\left[4 + \left(\frac{g}{2} + \mathrm{i}\sqrt{g}\right) e^{-\frac{\alpha}{\sqrt{m}}t\left(1+\frac{\mathrm{i}\sqrt{g}}{2}\right)} + \left(\frac{g}{2} - \mathrm{i}\sqrt{g}\right) e^{-\frac{\alpha}{\sqrt{m}}t\left(1-\frac{\mathrm{i}\sqrt{g}}{2}\right)}\right]. \tag{C.16}$$

Once the retarded Green's function of the system is known, the solution of the GLE (C.5) is straight forwardly computed by the convolution of the retarded Green's function and the inhomogeneity $\frac{\xi(t)}{m}$ of Eq. (C.5):

$$v(t) = \underbrace{\int_0^t G_{\mathrm{ret}}(t-t')\frac{\xi(t')}{m}\mathrm{d}t'}_{:=v_\xi(t)} + \underbrace{G_{\mathrm{ret}}(t)v(0)}_{:=v_a(t)}. \tag{C.17}$$

Given this solution, another specialty of dissipation kernel (C.1) can be derived. By computing $\langle v^2(t)\rangle$ in the limit $t \to \infty$ it appears that the usual form of the equipartition theorem in one dimension, given by

$$\lim_{t\to\infty} \frac{1}{2} m \langle v^2(t)\rangle = \frac{k_{\mathrm{B}}T}{2}, \tag{C.18}$$

no longer holds. Squaring and subsequently averaging of Eq. (C.17) leads to

$$\langle v^2(t)\rangle = \langle v_\xi^2(t)\rangle + \langle v_a^2(t)\rangle, \tag{C.19}$$

where the mixed terms vanish as the initial velocity v_0 and the noise $\xi(t)$ are uncorrelated, i.e. $\langle v(0)\xi(t)\rangle = 0$. In what follows, the values of both terms on the right-hand side of Eq. (C.19) are calculated separately.

Starting with $\langle v_\xi^2(t)\rangle$ the following computations have to be performed:

$$\begin{aligned}
\langle v_\xi^2(t)\rangle &= \frac{1}{m^2}\int_0^t \mathrm{d}t' \int_0^t \mathrm{d}t'' G_{\mathrm{ret}}(t-t')G_{\mathrm{ret}}(t-t'')\langle \xi(t')\xi(t'')\rangle \\
&= \frac{k_{\mathrm{B}}T}{m^2}\int_0^t \mathrm{d}t' \int_0^t \mathrm{d}t'' G_{\mathrm{ret}}(t-t')G_{\mathrm{ret}}(t-t'')\Gamma(|t'-t''|) \\
&= \frac{k_{\mathrm{B}}T}{m^2}\int_0^t \mathrm{d}\tau' \int_0^t \mathrm{d}\tau'' G_{\mathrm{ret}}(\tau')G_{\mathrm{ret}}(\tau'')\Gamma(|\tau''-\tau'|) \\
&= \frac{k_{\mathrm{B}}T}{m^2}\int_0^t \mathrm{d}\tau' \int_0^t \mathrm{d}\tau'' G_{\mathrm{ret}}(\tau')G_{\mathrm{ret}}(\tau'') \\
&\times \left[\Theta(\tau'-\tau'') + \Theta(\tau''-\tau')\right]\Gamma(|\tau''-\tau'|) \\
&= 2\frac{k_{\mathrm{B}}T}{m^2}\int_0^t \mathrm{d}\tau' \int_0^{\tau'} \mathrm{d}\tau'' G_{\mathrm{ret}}(\tau')G_{\mathrm{ret}}(\tau'')\Gamma(|\tau'-\tau''|) \\
&= \frac{2k_{\mathrm{B}}T}{m^2}\frac{mg(8+g)}{2(4+g)^2} = \frac{g(8+g)}{(4+g)^2}\frac{k_{\mathrm{B}}T}{m}, \quad t\to\infty,
\end{aligned} \tag{C.20}$$

where $\tau' = t - t'$ and $\tau'' = t - t''$.

Furthermore, for $\langle v_a^2(t)\rangle$ the following expression is obtained in the limit of $t \to \infty$:

$$\langle v_a^2(t)\rangle = G_{\mathrm{ret}}^2(t)\langle v^2(0)\rangle = \frac{16}{(4+g)^2}\langle v^2(0)\rangle, \quad t\to\infty. \tag{C.21}$$

Bringing together both solutions results in

$$\begin{aligned}
\lim_{t\to\infty}\langle v^2(t)\rangle &= \lim_{t\to\infty}\left(\langle v_\xi^2(t)\rangle + \langle v_a^2(t)\rangle\right) \\
&= \frac{g(8+g)}{(4+g)^2}\frac{k_{\mathrm{B}}T}{m} + \frac{16}{(4+g)^2}\langle v^2(0)\rangle,
\end{aligned} \tag{C.22}$$

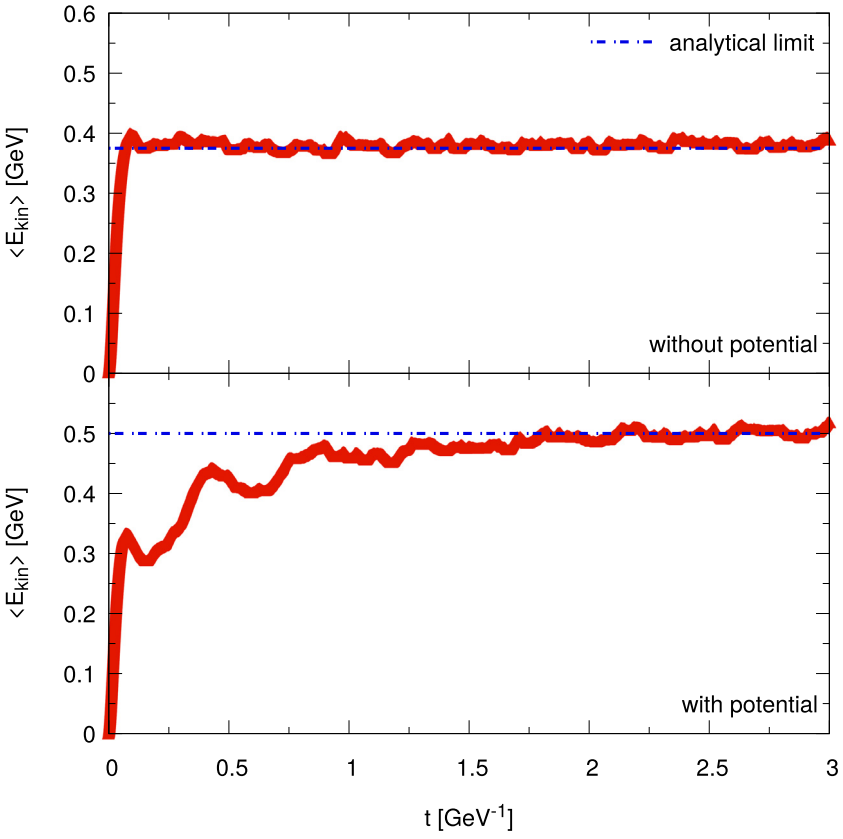

Fig. C.17. Average kinetic energy $\langle E_{\text{kin}}(t)\rangle$ with harmonic potential $V(x) = \frac{1}{2}m\omega_a^2 x^2$ (lower figure) and without potential (upper figure) as a function of the time t and its limit for $t \to \infty$ (blue dotted dashed line, see Eq. (C.18) or (C.23)), where $g = 4$, $m = 0.1\,\text{GeV}$, $k_B = 1$, $T = 1\,\text{GeV}$, $v_0 = 0$, $\omega_a = 10\,\text{GeV}$ (lower figure), and time step $\Delta t = 3.1 \cdot 10^{-5}\,\text{GeV}^{-1}$.

corresponding to the following mean kinetic energy in the limit of $t \to \infty$

$$\lim_{t\to\infty} \frac{1}{2} m \left\langle v^2(t)\right\rangle = \frac{g(8+g)}{(4+g)^2}\frac{k_B T}{2} + \frac{8m}{(4+g)^2}\left\langle v^2(0)\right\rangle. \tag{C.23}$$

Fig. C.17 shows that the numerical simulations in fact yield the analytically expected behavior of the kinetic energy in the limit of $t \to \infty$.

Investigating furthermore the velocity distribution function it appears that thermal equilibrium is established but with a temperature reduced by approximately a factor $\frac{g(8+g)}{(4+g)^2}$, which is the coefficient of the first term in Eq. (C.23) (see Fig. C.18). Based on these considerations an effective temperature T_{eff} can be defined as

$$T_{\text{eff}} = \frac{g(8+g)}{(4+g)^2} T. \tag{C.24}$$

This pathological behavior of insufficient thermalization directly stems from the fact that the Fourier transform, $\tilde{\Gamma}(\omega)$ (see Eq. (C.2)), of correlation function C_3 vanishes in the limit of $\omega \to 0$. In contrast, for a Brownian particle trapped in a standard oscillator potential, one can analytically prove that the particle thermalizes for the kinetic as well as for the potential energy. Numerical simulations of such a Brownian particle, originally trapped at the bottom of a harmonic potential $V(x) = \frac{1}{2}m\omega_a^2 x^2$,

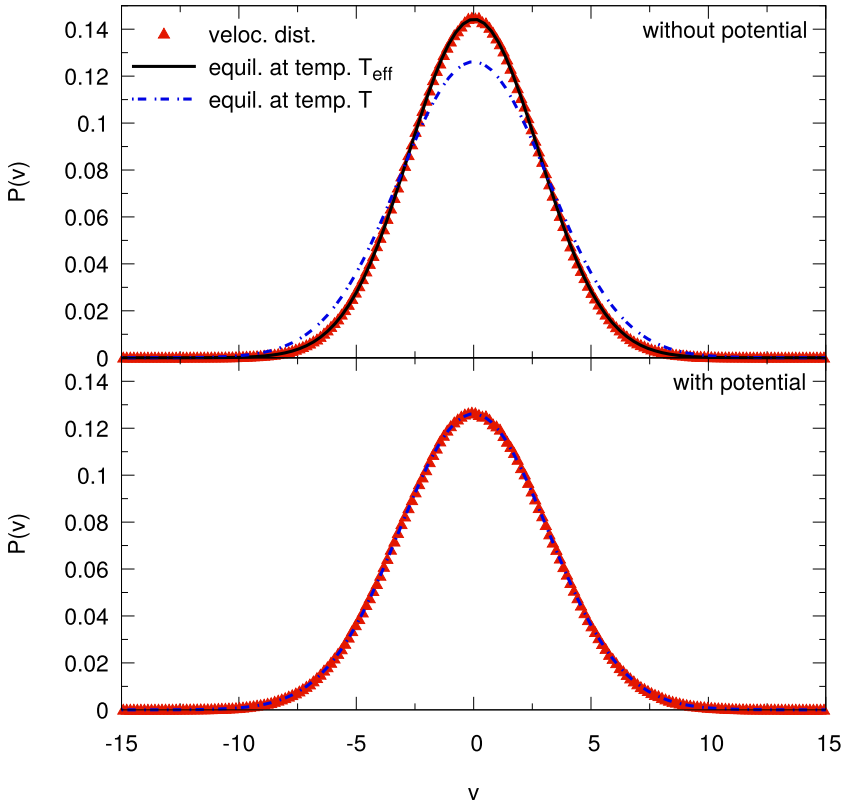

Fig. C.18. Velocity distribution $P(v)$ (red triangles) with harmonic potential $V(x) = \frac{1}{2} m \omega_a^2 x^2$ (lower figure) and without potential (upper figure) and the equilibrium distributions for temperature T_{eff} (black line) (see Eq. (C.24)) and temperature T (blue dotted dashed line), where $g = 4$, $m = 0.1\,\text{GeV}$, $k_B = 1$, $T = 1\,\text{GeV}$, $v_0 = 0$, $\omega_a = 10\,\text{GeV}$ (lower figure), and time step $\Delta t = 3.1 \cdot 10^{-5}\,\text{GeV}^{-1}$.

indeed show that the usual form of the equipartition theorem (see Eq. (C.18)) is again valid and thermal equilibrium with temperature T instead of T_{eff} is recovered (see Fig. C.18). In an analogous manner the retarded Green's function for the position $x(t)$ will contain poles below the real axis at $\omega = \pm\omega_a$. For weak coupling the effective damping is then obtained by $\tilde{\Gamma}(\omega = \omega_a)/2$ in the linear harmonic (or quasi-particle) approximation [11,13,14].

References

[1] A. Einstein, Ann. Phys. 322 (1905) 549, URL http://dx.doi.org/10.1002/andp.19053220806.
[2] P. Langevin, C. R. 146 (1908) 530–533.
[3] D.S. Lemons, A. Gythiel, P. Langevin's, Amer. J. Phys. 65 (1997) 1079–1081, URL https://doi.org/10.1119%2F1.18725.
[4] W.T. Coffey, Y.P. Kalmykov, J.T. Waldron, The Langevin Equation: With Application to Stochastic Problems in Physics, Chemistry and Elctrical Engineering, second ed., in: World Scientific Series in Contemporary Chemical Physics, vol. 14, World Scientific, Singapure, 2004.
[5] A.O. Caldeira, A.J. Leggett, Phys. Rev. Lett. 46 (1981) 211, URL http://dx.doi.org/10.1103/PhysRevLett.46.211.
[6] A.O. Caldeira, A.J. Leggett, Ann. Physics 149 (1983) 374, URL http://dx.doi.org/10.1016/0003-4916(83)90202-6.
[7] U. Weiss, Quantum Dissipative Systems, second ed., World Scientific, Singapore, New Jersey, London, Hong Kong, 1999.
[8] E.A. Calzetta, B.L. Hu, Nonequilibrium Quantum Field Theory, Cambridge University Press, Cambridge, New York, Melbourne, Madrid, Cape Town, Singapore, Sao Paulo, Delhi, 2008.
[9] M. Gleiser, R.O. Ramos, Phys. Rev. D 50 (1994) 2441.

[10] J. Knoll, D.N. Voskresensky, Ann. Physics 249 (1996) 532, URL http://dx.doi.org/10.1006/aphy.1996.0082.
[11] C. Greiner, B. Müller, Phys. Rev. D 55 (1997) 1026–1046.
[12] D.H. Rischke, Phys. Rev. C 58 (1998) 2331–2357.
[13] C. Greiner, S. Leupold, Ann. Phys. 270 (1998) 328–390, URL http://dx.doi.org/10.1006/aphy.1998.5849.
[14] Z. Xu, C. Greiner, Phys. Rev. D 62 (2000) 036012, URL http://dx.doi.org/10.1103/PhysRevD.62.036012.
[15] R.L.S. Farias, R.O. Ramos, L.A. da Silva, Phys. Rev. E 80 (2009) 031143.
[16] J. Dunkel, P. Hänggi, Phys. Rep. 471 (2009) 1.
[17] R.L.S. Farias, R.O. Ramos, L.A. da Silva, Braz. J. Phys. 38 (2008) 499.
[18] R. Rapp, H. van Hees, in: R.C. Hwa, X.-N. Wang (Eds.), Quark Gluon Plasma 4, World Scientific, 2009, p. 111, URL http://arxiv.org/abs/0903.1096.
[19] A. Andronic, et al., Eur. Phys. J. C 76 (2016) 107.
[20] M. Nahrgang, S. Leupold, C. Herold, M. Bleicher, Phys. Rev. C 84 (2011) 024912, URL http://dx.doi.org/10.1103/PhysRevC.84.024912.
[21] C. Herold, M. Nahrgang, I. Mishustin, M. Bleicher, Phys. Rev. C 87 (2013) 014907, URL http://dx.doi.org/10.1103/PhysRevC.87.014907.
[22] J.I. Kapusta, C. Young, Phys. Rev. C 90 (2014) 044902.
[23] P. Hänggi, F. Mojtabai, Phys. Rev. A 26 (1982) 1168, URL https://link.aps.org/doi/10.1103/PhysRevA.26.1168.
[24] P. Hänggi, J. Stat. Phys. 30 (1983) 401.
[25] U. Seifert, S. Dietrich, Europhys. Lett. (EPL) 3 (1987) 593, URL https://doi.org/10.1209/0295-5075/3/5/013.
[26] J.H.v. Hoff, Etudes de Dynamique Chimique, Frederik Muller, Amsterdam, 1884.
[27] Arrhenius, Z. Phys. Chem. 4 (1889) 226.
[28] P. Hänggi, P. Talkner, M. Borkovec, Rev. Modern Phys. 62 (1990) 251, URL https://link.aps.org/doi/10.1103/RevModPhys.62.251.
[29] H. Kramers, Physica 7 (1940) 284, URL http://www.sciencedirect.com/science/article/pii/S0031891440900982.
[30] B. Schüller, Kramers's Escape Rate Problem with Regard to Non-Markovian Noise (Master's thesis), Johann Wolfgang Goethe-Universität, 2018.
[31] J. Schmidt, A. Meistrenko, H. van Hees, Z. Xu, C. Greiner, Phys. Rev. E 91 (2015) 032125.
[32] T.F. Hannes Risken, The Fokker–Planck Equation: Methods of Solution and Applications, second ed., in: Springer Series in Synergetics, Springer, 1996.
[33] C. Heer, Statistical Mechanics, Kinetic Theory, and Stochastic Processes, Academic Press, 1972.
[34] B. Carmeli, A. Nitzan, Phys. Rev. A 29 (1984) 1481, URL https://link.aps.org/doi/10.1103/PhysRevA.29.1481.
[35] B.J. Matkowsky, Z. Schuss, C. Tier, J. Stat. Phys. 35 (1984) 443, URL https://doi.org/10.1007/BF01014395.
[36] A.G. Zawadzki, J.T. Hynes, Chem. Phys. Lett. 113 (1985) 476, URL http://www.sciencedirect.com/science/article/pii/0009261485800841.
[37] J.E. Straub, M. Borkovec, B.J. Berne, J. Chem. Phys. 84 (1986) 1788.
[38] H. Brinkman, Physica 22 (1956) 149, URL http://www.sciencedirect.com/science/article/pii/S0031891456800190.
[39] R. Landauer, J.A. Swanson, Phys. Rev. 121 (1961) 1668, URL https://link.aps.org/doi/10.1103/PhysRev.121.1668.
[40] P. Talkner, E. Pollak, Phys. Rev. E 47 (1993) R21, URL https://link.aps.org/doi/10.1103/PhysRevE.47.R21.
[41] E. Pollak, P. Talkner, Phys. Rev. E 47 (1993) 922, URL https://link.aps.org/doi/10.1103/PhysRevE.47.922.
[42] P. Talkner, Anharmonic Barrier Corrections for Kramers' Rate-Problem in the Spatial Diffusion Regime, Springer Netherlands, Dordrecht, 1995, URL https://doi.org/10.1007/978-94-011-0465-4_3.
[43] E.V. Sukhorukov, A.N. Jordan, Phys. Rev. Lett. 98 (2007) 136803, URL https://link.aps.org/doi/10.1103/PhysRevLett.98.136803.
[44] H. Grabert, Phys. Rev. B 77 (2008) 205315, URL https://link.aps.org/doi/10.1103/PhysRevB.77.205315.
[45] A. Baura, M.K. Sen, G. Goswami, B.C. Bag, J. Chem. Phys. 134 (2011) 044126, URL https://doi.org/10.1063/1.3521394.
[46] S. Ishioka, J. Phys. Soc. Japan 48 (1980) 367.
[47] P.G. Wolynes, Phys. Rev. Lett. 47 (1981) 968, URL https://link.aps.org/doi/10.1103/PhysRevLett.47.968.
[48] E. Cortés, B.J. West, K. Lindenberg, J. Chem. Phys. 82 (1985) 2708.
[49] B. Carmeli, A. Nitzan, J. Chem. Phys. 79 (1983) 393.
[50] R.F. Grote, J.T. Hynes, J. Chem. Phys. 77 (1982) 3736, URL https://doi.org/10.1063/1.444277.
[51] S.A. Adelman, J. Chem. Phys. 64 (1976) 124.
[52] R.L.B.J.D. Faires, Numerical Methods, Brooks/ Cole-Thomson Learning, 2003.
[53] I. Gontchar, M. Chushnyakova, Pramana - J. Phys. 88 (2017).
[54] D. Boilley, Y. Lallouet, J. Stat. Phys. 125 (2006) 473, URL http://dx.doi.org/10.1007/s10955-006-9197-5.
[55] P.P.G. Dyke, An Introduction to Laplace Transforms and Fourier Series, Springer, 1999.
[56] G. Doetsch, Introduction to the Theory and Application of the Laplace Transformation, second ed., Springer-Verlag, 1974.
[57] W. Greiner, Classical Mechanics: Systems of Particles and Hamiltonian Dynamics, second ed., Springer-Verlag Berlin Heidelberg, 2010.